Tke5 is a novel *Pseudomonas putida* toxin that depolarises membranes killing plant pathogens

Carmen Velázquez[1,†], Alejandro Arce-Rodríguez[2,†], Jon Altuna-Alvarez[1], Jessica Rojas-Palomino[3], Andony Flores-Ceron[2], Citlaly Cando[2], Adrián Ruiz[2], Amaia González-Magaña[1], María Queralt-Martín[3], Antonio Alcaraz[3], David Albesa-Jové[1,4*] and Patricia Bernal[2*]

[1]Instituto Biofisika (CSIC, UPV/EHU), Fundación Biofísica Bizkaia/Biofisika Bizkaia Fundazioa (FBB), 48940, Leioa, Spain

Departamento de Bioquímica y Biología Molecular, University of the Basque Country, 48940, Leioa, Spain

[2]Departamento de Microbiología, Facultad de Biología, Universidad de Sevilla, 41012, Seville, Spain

[3]Laboratory of Molecular Biophysics, Department of Physics, University Jaume I, 12071, Castellón, Spain

[4]Ikerbasque, Basque Foundation for Science, 48013 Bilbao, Spain.

*For correspondence: david.albesa@ehu.eus and pbernal@us.es

[†]These authors have contributed equally to this work.

Running title: Tke5: A new weapon in the *P. putida* arsenal

Keywords: Type VI secretion systems, toxins, immunity proteins, bacterial membranes, plant pathogens, biological control agent, *Pseudomonas putida*

Abbreviations: T6SS, Type VI secretion system; EI pair, effector-immunity pair; UV, ultraviolet; CDD, Conserved Domain Database; 3-*m*Bz, 3-methyl-benzoate; IPTG, β-D-1-thiogalactopyranoside; CFU, colony-forming units.

Authors Note: Two datasets, three supplementary figures and three supplementary tables are attached.

ABSTRACT

The soil bacterium *Pseudomonas putida* injects toxic proteins into neighbouring competitors including resilient phytopathogens using the Type VI secretion system (T6SS). The secretion of toxins endows *P. putida* a significant fitness advantage, allowing this biocontrol agent to thrive in plant-related polymicrobial environments and prevent phytopathogen infections. However, despite the significance of *P. putida* in agriculture and biotechnology, the identity and mechanisms of action of most of its toxins remain largely unexplored. This is in part because only one of the three T6SSs identified in *P. putida* (K1-T6SS) is active under laboratory conditions, limiting the study of toxins secreted through the K2- and K3-T6SSs. We present the first comprehensive molecular characterisation of Tke5, a potent toxin encoded within the K3-T6SS, which represents the first functional analysis of the BTH_I2691 protein family within the cl49522 superfamily. Our findings reveal that Tke5 is a novel pore-forming toxin that disrupts bacterial membranes through selective ion transport rather than by forming large, non-specific membrane disruptions. This mechanism leads to membrane depolarisation and bacterial cell death while preserving overall membrane integrity, distinguishing it from conventional detergent-like pore-forming toxins. This discovery not only contributes to our fundamental understanding of a widespread yet understudied toxin family, but also introduces a powerful new mechanism for targeting even the most resilient phytopathogens, potentially revolutionising the biocontrol capabilities of *P. putida*. Our work highlights the importance of studying bacterial toxins in the context of biocontrol, offering alternatives to combat plant pathogens without relying on traditional chemical pesticides.

INTRODUCTION

Toxins are biochemical substances that can cause disease, death or cellular damage when introduced into or produced within an organism. They interfere with vital cellular processes such as inhibiting enzymatic activities or disrupting metabolism, protein biosynthesis or membrane functions. Among these diverse toxic substances, pore-forming toxins (PFTs) represent a particularly sophisticated class of molecular weapons that have evolved across multiple domains of life, being produced by various organisms including bacteria, archaea, protozoans, vertebrates or plants [1,2]. PFTs create pores in target cell membranes, leading to an influx or efflux of ions, small molecules, or proteins through the host membrane, triggering various secondary responses including cell death or more subtle manipulation of cell function [3]. PFTs are broadly classified into two categories based on the secondary structures that form the pore: α-PFTs use α-helices to form the transmembrane pore such as colicins, cytolysin A (ClyA), and actinoporins; and β-PFTs utilise β-sheets/β-barrels to form the pore, which includes *Staphylococcus aureus* α-hemolysin, anthrax toxin or streptolysin O [1,3]. PFTs are soluble proteins that must undergo a transition from the soluble state into a membrane-spanning structure. They bind to the membrane of target cells via specific receptors or non-specific associations with the lipid bilayer. Upon membrane binding, PFT monomers oligomerise, inserting a specific pore-forming motif into the membrane to create a water-filled transmembrane pore. The structural complexity of these pores is evident in their stoichiometry and size, which can vary dramatically: from tetramers to structures involving 50 or more monomers. Consequently, pore dimensions range widely, from as small as 1-2 nm in small β-PFTs to more than 50 nm for large β-PFTs such as the cholesterol-dependent cytolysins (CDCs). The insertion process typically involves significant conformational changes in the protein structure, reflecting the

dynamic nature of these molecular pore-forming mechanisms. These toxins can show distinct ion preferences, with channels formed by C2 toxin being cation-selective, while aerolysin and epsilon-toxin channels are anion-selective [1,3]. Some PFTs, such as *P. aeruginosa* Tse5 have a multi-ionic character, exhibiting a preference for cations while remaining permeable to anions [4,5].

In bacterial contexts, toxins such as PFTs are often proteins secreted or injected into target cells as part of complex molecular mechanisms of defence or competition and are designed to target eukaryotic host cells or act against rival microorganisms, killing (bactericidal effect) or inhibiting the growth (bacteriostatic) of competing microorganisms. The type VI secretion system (T6SS) represents one of the best-characterised bacterial weapon systems, primarily deploying antimicrobial compounds against Gram-negative bacteria [6]. Its structural components include a cell wall-anchored membrane complex, a baseplate, a contractile sheath-tube assembly, and a spike. Effector proteins are loaded onto specific components, such as the inner Hcp tube and the VgrG-PAAR spike complex, and are ejected upon sheath contraction [7–13]. To ensure loading, T6SS effectors utilise specialised delivery mechanisms. Some effectors are encased in protective Rhs shells, while others rely on chaperones or adaptor proteins like EagR and Tap. T6SS effector genes typically cluster near structural component genes (*vgrG*, *PAAR*, *hcp*) and are often accompanied by their chaperone and adaptor genes. Recent research has identified effector-specific motifs (MIX, FIX, RIX, PIX) that are primarily N-terminal domains that facilitate the transport of the C-terminal toxic domain into target cells via the T6SS [14–18].

The production of protein toxins by bacteria for competitive advantage comes with a significant challenge: avoiding self-harm. To address this, toxin-producing bacteria have evolved a sophisticated self-protection mechanism. They produce specific immunity

proteins that neutralise the effects of their own toxins, creating a crucial safeguard against self-intoxication. These immunity proteins are typically encoded immediately downstream of the toxin gene, forming a toxin-immunity pair. This genetic organisation serves two important functions: it ensures the simultaneous production of both the toxin and the cognate immunity protein, and it allows for the modular integration of the toxin-immunity pairs into diverse secretion systems [19]. While the exact mechanisms of immunity against PFTs are not fully understood, the immunity proteins for these toxins are usually small and hydrophobic, indicating that they likely localise to the cytoplasmic membrane. At this location, they may interfere with pore opening or disrupt the oligomerisation process of the pore-forming toxins [19].

The potent antibacterial activity of toxins has led to the exploration of their use in biological control. Many beneficial bacteria, such as some *Pseudomonas* species, act as effective biocontrol agents (BCAs) due to their ability to produce toxins that can inhibit or kill plant pathogens. Biocontrol is of significant importance in modern agriculture, offering a sustainable and environmentally friendly alternative to traditional chemical pesticides. The understanding of the underlying mechanisms of toxins, including PFTs could enhance the development of effective BCAs. In *P. putida*, a plant growth-promoting rhizobacteria (PGPR) well known for its biocontrol ability [20], the T6SS is instrumental in the elimination of severe plant pathogens [21]. *P. putida* KT2440 possesses three T6SSs (K1-, K2- and K3-T6SS) and their associated toxins [21], with predicted functions such as nucleases (Tke2, Tke4 and Tke10), pore-forming colicins (Tke6, Tke7, Tke8) or NAD^+/$NADP^+$ hydrolases *i.e.* Tke1. However, no predicted functions exist for putative Tke5, Tke9 and Tke3 effectors and more importantly, none of the nine T6SS toxins of this strain have been characterised. Additionally, while the regulation of the K1-T6SS cluster has been thoroughly investigated [21,22], nothing is known about

secretion through the K3-T6SS and its predicted associated effector Tke5. The primary reason for this lack of knowledge is that K3-T6SS is silenced under laboratory conditions [21,22] limiting the study of its components.

Advancing our understanding of novel toxins and their molecular mechanisms remains crucial for developing effective biocontrol strategies in sustainable agriculture. In this context, our work reveals the mechanism of action of Tke5, a putative T6SS effector of the biocontrol agent *P. putida*, providing the first functional characterisation of the BTH_I2691 protein family within the cl49522 superfamily. Tke5 forms selective nanometric pores in the cytoplasmic membrane of target cells, disrupting cellular homeostasis through cell depolarisation without compromising membrane integrity. This discovery not only contributes to our fundamental understanding of bacterial competition, but the potent bactericidal activity of Tke5 against phytopathogens also opens new avenues for developing more effective and environmentally friendly crop protection strategies.

METHODS

Bacterial strains and growth conditions

Bacterial strains are listed in Table S1. Unless otherwise stated, chemicals and reagents, including antibiotics, were purchased from Sigma Aldrich. All strains were grown in Lysogeny broth (LB Lennox; 5 g L^{-1} NaCl) and agar (1.5% w/v) [23] for routine growth with shaking at 180 rpm, as appropriate. *E. coli* strains were incubated at 37°C, phytopathogens at 28ºC and *P. putida* strains at 30°C. Vogel-Bonner Medium (VBM) (200 mg L^{-1} $MgSO_4 \cdot 7H_2O$; 2 g L^{-1} anhydrous citric acid; 10 g L^{-1} K_2HPO_4; 3.5 g L^{-1} $NaNH_4HPO_4 \cdot 4H_2O$; pH 7.0) was used to select transconjugants after triparental

conjugation, as *E. coli* donor and helper cells cannot grow using citrate as carbon source. Antibiotics were used at the following concentrations (µg mL^{-1}): rifampicin (Rif), 20 for *P. putida*; kanamycin (Km), 50 for *P. putida*, *Agrobacterium tumefaciens*, *Pectobacterium carotovorum*, *Pseudomonas savastanoi*, *Pseudomonas syringae* and *Dickeya dadantii*, 25 for *E. coli* and *Ralstonia solanacearum*, and 20 for *Xanthomonas campestris*; ampicillin (Amp) 100 for *E. coli*, gentamycin (Gm), 25 for *P. putida* and 15 for *E. coli*; chloramphenicol (Cm), 10 for *E. coli;* nalidixic acid (Nal), 10 for *E. coli;* streptomycin (Sm), 50 for *E. coli.*

Construction of plasmids and bacterial strains

Plasmids and primers used in this study are listed in Tables S2 and S3. DNA manipulations were performed using standard methods [23]. Q5® High-Fidelity DNA polymerase (New England Biolabs) was used for PCR reactions according to the manufacturer's instructions. Primers were synthesised by Macrogen Inc. and restriction enzymes were purchased from New England Biolabs. Plasmid isolation and purification of PCR products were performed with the Plus SV Miniprep DNA Purification System and the Gel and PCR Clean-Up System (Promega) respectively. All DNA constructs were sequenced and verified to be correct before use.

Recombinant plasmids were transferred to *E. coli* strains by transformation and to *Pseudomonas*, *Ralstonia*, *Agrobacterium*, *Dickeya*, *Pectobacterium*, *Erwinia* and *Xanthomonas* strains by electroporation [24] or conjugation [25], as appropriate.

The *tke5* (PP2612) gene was amplified from genomic DNA extracted from *P. putida* KT2440 using primers P1-P2 and P3-P2 (Table S3). Primer P3 is designed to fuse a *pelB* signal sequence at the 5´end. This sequence encodes the 22 aminoacids, N-terminal leader peptide MKYLLPTAAAGLLLLAAQPAMA (UniProt Q04085) originally from

the Pectate lyase B (PelB) of *Erwinia carotovora* EC [26]. PelB directs the fused protein, Tke5, to the Sec pathway [27]. The *tke5* and *pelB-tke5* genes were cloned into pJET1.2/blunt (Thermo Scientific™), sequenced and then subcloned into the broad host range, medium copy number vector pS238D•M (Table S2, [28]) from the SEVA collection at the NheI/BamHI sites, which excise the *msfGFP* to produce pS238D•*tke5* or pS238D•*pelB-tke5*. Primers P4-P5 that bind up- and downstream pS238D•M insertion site were used to screen colonies harbouring the insert *pelB-tke5* and for subsequent sequencing.

The *tke5* gene was subcloned from pS238D•*tke5* to pCOLADuet™-1 into *mcs-2*, including the TAA stop codon to avoid fusion with the C-terminal S-tag. Subsequently, a tag coding for 9x His residues and a Tobacco Etch Virus (-TEV) cleavage site was cloned upstream *tke5*, resulting in vector pCOLADuet-1•*9xhis-tke5*. These constructs were produced by GenScript service (Table S2).

The *tki5* (PP2611) gene preceded by an artificial RBS region (TTTAAAGGAGATATACAA) was synthesised and cloned into pSEVA424 vector between the KpnI and HindIII restriction sites using GenScript service (Table S2). The RBS and the *tki5* gene were subcloned into the broad host range, low copy number vector pSEVA624C at the KpnI/HindIII sites to produce pSEVA624C•*tki5* (Table S2). Vector pSEVA624C is a derivative of pSEVA621 from the SEVA collection [29,30] constructed in this study where the *lacI*^{q}-P_{trc} cargo from pSEVA234C [31] was inserted in the *mcs* using PacI/HindIII. Primers P6-P7 were used to screen for the *lacI*^{q}-P_{trc} cargo insertion (Table S3) and primers P8-P9 which bind up- and downstream pSEVA624C *mcs* to screen colonies harbouring the insert *tki5* and for subsequent sequencing. Vector pSEVA624C has been deposited into NCBI Genbank with accession number PQ628036 and into the SEVA repository https://seva-plasmids.com/ [29,30].

Bioinformatic analysis

Pseudomonas tke5 and *tki5* gene sequences and their respective protein product Tke5 and Tki5 were obtained from the Pseudomonas Genome database [32].

Sequence homology search - Blast-P

BLASTP analyses were performed at the NCBI website using version 2.16.0 [33] and amino acid sequence searches using SMART [34] and Pfam [35] with the default settings.

Conserved Domain Database - CDD

The CDD from NCBI was used to visualise the conserved domains of proteins Tke5 and Tki5. We accessed this database directly from the output of the BLASTP analyses. The CDD includes NCBI-curated domains, which use 3D-structure information to explicitly define domain boundaries and provide insights into sequence/structure/function relationships, as well as domain models imported from external source databases including Pfam, SMART, COG, PRK and TIGRFAMs [36].

Protein Remote homology detection and 3D structure prediction - HHpred

Additionally, we have used the HHpred server to predict protein homology and 3D structure of Tke5 using the default parameters. This tool belongs to the Max Planck Institute (MPI) Bioinformatics Toolkit.

CDART

We used the Conserved Domain Architecture Retrieval Tool (CDART) from the NCBI website to visualise the different architectures present in the BTH_I2691 protein family. To do so, we introduce the accession number for this domain between brackets [NF041559] in the “Enter Query Protein Sequence” box under “Launch a new search” on the website of this tool. The output was downloaded in a comma-delimited table and is attached to this work as Dataset S1.

Topology –TMHMM-2.0

The topology of Tke5 and Tki5 was predicted using the TMHMM-2.0 algorithm (DTU Health Tech; [37]) with the default settings.

Phylogenetic tree

Protein sequences for phylogenetic analysis were retrieved from the NCBI website after the BLAST-P analysis. The multi-FASTA file was loaded in the Molecular Evolutionary Genetic Analysis (MEGA) tool version 11 [38] for alignment using the ClustalW algorithm. The resulting .mas file was exported as .mega to perform the evolutionary analysis by the Maximum Likelihood method with 500 bootstrap replications and JTT matrix-based model [39] using the same software (MEGA11), exact details as follow as stated in the software after analysis:

"The evolutionary history was inferred by using the Maximum Likelihood method and JTT matrix-based model [39]. The tree with the highest log likelihood (-133685.63) is shown. Initial tree(s) for the heuristic search were obtained automatically by applying Neighbor-Join and BioNJ algorithms to a matrix of pairwise distances estimated using the JTT model, and then selecting the topology with superior log likelihood value. The tree is drawn to scale, with branch lengths measured in the number of substitutions per site. This analysis involved 71 amino acid sequences. There were a total of 1566 positions in the final dataset. Evolutionary analyses were conducted in MEGA11 [38]".

The resulting file (.mtsx) was exported to a Newick file and loaded into iTOL software [40] for annotation and personalisation at the visualisation level.

Structural-base homology search and protein interactions prediction

- **AlphaFold and Foldseek**

The structure of Tke5 was predicted using AlphaFold2 and the PDB file was used as a query to search for homologues based on the structure using Foldseek Search Tool [41] with the default settings.

Multiple Sequence Alignment (MSA) - Clustal Omega and Jalview

VasX from *V. cholerae* serotype O1 (strain ATCC 39315/ El Tor Iaba N16961) with the following identifiers: locus VC_A0020; Uniprot: Q9KNE5 VASX_VIBCH and Tke5 (PP2612) from *P. putida* KT2440 were aligned using the Multiple Sequence Alignment (MSA) tool of Clustal Omega (EMBL-EBI) [42] with the default settings and Jalview software was used to visualise the alignment (Supplementary Fig. 1). ChimeraX [43] was used for the visualisation of the AlphaFold predicted 3D structure of Tke5 and VasX.

Growth inhibition and immunity-driven recovery assays

Cells of *P. putida* KT2440 were electroporated as previously described with a combination of the two compatible plasmids pS238D•M and pSEVA624C or their derivates harbouring *tke5* or *pelB-tke5* and *tki5*, respectively, as described in Table S2. LB-agar supplemented with Km and Gm was used to select successfully transformed cells. The presence of the plasmid was corroborated by colony PCR using primers P4-P5 and P8-9 (Table S3) for pS238D•M and pSEVA624C derivatives, respectively.

To perform the growth curves, overnight cultures of each strain were grown in LB supplemented with the appropriate antibiotics. The next day, the cultures were adjusted to OD_{600} 0.05 in the same medium, and 1 mM of β-D-1-thiogalactopyranoside (IPTG) was added to induce *tki5*. Aliquots of 200 µL were placed in a microtiter plate and the Synergy/H1 microplate reader (Biotek©) was used to measure the OD_{600} every 15 min at 30 ºC. After an initial incubation of 2 h, 0.5 mM of 3-methylbenzoate (3-*m*Bz) was

added to each well and cultivated for another 14 h. Data was obtained for three biological replicates, each with technical duplicates.

Survival growth in the presence of antimicrobial compounds

Overnight cultures of *E. coli* DH5α harbouring the vector pS238D•M [28] or the derivate encoding the PelB-Tke5 effector (pS238D•*pelB-tke5*, Table S2) were grown in LB medium supplemented with Km and diluted in 20 mL of the same medium at OD_{600} of 0.1. A 25 µL sample of each culture was taken at timepoint zero to quantify colony-forming units (CFU) as described below. When required, expression of *pelB-tke5* was induced with 0.5 mM 3-*m*Bz. A bactericidal (Gm_{10}) or a bacteriostatic (Tc_5) antibiotic was added to cultures of the control strain *E. coli* pS238D•M for reference to different substances affecting bacterial growth. The cultures were incubated at 30 ºC/180 rpm for 6 h, 25 µL samples were taken every hour and serial dilutions from 10^{-1} to 10^{-6} were prepared in a microtiter plate with phosphate buffered saline (PBS). A 20 µL aliquot of each dilution was placed onto 120 mm square LB-agar plates in technical duplicates. CFU were determined after 24 and 48h of incubation at 37 ºC. The survival ratio was calculated based on the difference in CFU between each timepoint and timepoint zero expressed as CFUt=x/CFUt=0. Cellular survival was represented as the Log_{10} of the survival ratio. Three biologically independent experiments were performed.

Flow cytometry studies of* E. coli *DH5α cells expressing tke5, pelB-tke5, and tki5

Overnight cultures of *E. coli* DH5α alone or harbouring the vector pS238D (Calles et al., 2019), its derivate encoding the Tke5 (pS238D•*tke5*, Table S2) or PelB-Tke5 effector (pS238D•*pelB-tke5*, Table S2) and pSEVA624C•*tki5*, were grown in LB medium and supplemented with Km and Gm when appropriated. Genes *tke5* and *pelB-tke5* were induced with 1 mM 3-*m*Bz when the cultures reached OD_{600} of 0.6 and

incubated for 2 additional hours in the same conditions. Immunity gene *tki5* was induced with 1 mM IPTG for 1 hour before the 3-*m*Bz induction of the effector gene *tke5*. To avoid the leaking expression of the P_{trc}, 0.2% glucose was added to the strains harbouring the pSEVA624C•*tki5* vector. Cultures were diluted in 10 mL of the same medium at OD_{600} of 0.05 and incubated for 2 hours once the 3-*m*Bz was added. Then, bacterial cultures were centrifugated at 6000 g for 15 min at 4 ºC. To perform the flow cytometry studies, the bacterial pellets were resuspended in 1x PBS solution pH 7.4 to reach a final OD_{600} of 0.5.

To establish control populations, *E. coli* DH5α cells were subjected to heat shock at 85 °C for 5 minutes followed by cooling at 4 °C for 2 minutes and stained with 4 μM of the fluorescent dye Sytox™ Deep Red to identify the permeabilised population. For the depolarised population, *E. coli* DH5α cells were treated with the antibiotic polymyxin B sulfate (100 μg mL^{-1}) for 30 min and stained with 10 μM of the fluorescent dye $DiBAC_4(3)$. Additionally, *E. coli* DH5α cells harbouring the pS238D vector, with and without 3-*m*Bz induction, were incubated with $DiBAC_4(3)$ and Sytox™ Deep Red to serve as controls for the healthy population (Supplementary Fig. 2a-d). Cells were incubated with the fluorescent dyes for 45 min under constant shaking in dark conditions. Data was collected in the CytoFLEX cytometer with 488 and 638 nm lasers. Channels selected were FITC and APC for $DiBAC_4(3)$ (Exλ = 490 nm, Emλ = 516 nm) and Sytox™ Deep Red (Exλ = 660 nm, Emλ = 682 nm), respectively.

E. coli DH5α strains harbouring either pS238D•*tke5* or pS238D•*pelB-tke5* or co-transformed with pS238D•*pelB-tke5* and pSEVA624C•*tki5* to assess the neutralisation effect of the immunity gene are shown in Supplementary Fig. 2e-h. Each measurement was performed in triplicate to determine the mean value, and each condition was tested

in tree-independent experiments (n=3). All data were subsequently analysed using CytExpert.

Expression and purification of Tke5 to study pore-formation in lipid bilayers

Escherichia coli BL21(DE3) cells co-transformed with the pCOLADuet-1•*9xhis-tke5* and pSEVA624C•*tki5* plasmids were grown overnight at 37 °C with agitation in 200 mL of LB media supplemented with Km and Gm. For Tke5/Tki5 expression, bacterial cultures were diluted to an initial OD_{600} of 0.1 in 2 L of fresh LB medium supplemented with Km and Gm and induced when the OD_{600} reached 0.7 by adding IPTG to a final concentration of 1 mM. The temperature was lowered to 18 °C, and the bacterial cultures were left overnight in shaking conditions. Cells were harvested by centrifugation at 6000 × g for 20 min, and pellets were stored at −80 °C for subsequent use.

The pellet from 4 L of bacterial culture was resuspended in 60 mL of 50 mM Tris–HCl pH 8.0, 500 mM NaCl, 20 mM imidazole (solution A) along with 5 µL of benzonase endonuclease (Millipore, Sigma) and a tablet of protease inhibitor cocktail (cOmplete, EDTA-free, Roche). Cell lysis was performed using sonication with continuous cycles of 15 s ON and 59 s OFF at 60 % amplitude, followed by ultracentrifugation at 125,748 × g for 1 hour. The supernatant was filtered through a 0.2 µm membrane and then loaded via a peristaltic pump onto a 5-ml HisTrap HP column (GE Healthcare) equilibrated with solution A.

The column was connected to a fast protein liquid chromatography system (ÄKTA FPLC; GE Healthcare) and washed with solution A at 1 mL min^{-1} until the absorbance at 280 nm approached baseline. Tke5 was eluted using 100% solution B (50 mM Tris–HCl pH 8, 500 mM NaCl and 500 mM imidazole) at 3 mL min^{-1}. The central peak fractions were combined, and dithiothreitol (DTT) was added to a final concentration of

2 mM. The protein solution was injected into a HiLoad Superdex 200 26/600 pg column, previously equilibrated with 20 mM Tris–HCl pH 8, 150 mM NaCl and 2 mM DTT (solution C). Tke5 eluted as a single monodispersed protein, appearing as a unique band on an SDS–PAGE gel (Supplementary Fig. 3). The identity of the Tke5 band was confirmed by mass spectrometry (Dataset S2). Peak fractions were pooled and concentrated using Amicon centrifugal filter units (30 kDa molecular mass cut-off, Millipore) to a final concentration of 2.5 mg mL^{-1} (*ca*. yield: 1.5 mg L^{-1}) to perform lipid bilayer experiments.

Study of Tke5 pore-forming activity in planar lipid bilayers

We used the solvent-free modified Montal-Mueller technique to enable the formation of planar lipid membranes in the orifice made over a Teflon film [44]. Lipid preparation involved chloroform evaporation of *E. coli* polar lipid extract (Avanti Polar Lipids; Alabaster, AL) under an argon stream, followed by dissolution in pentane at a concentration of 5 mg mL^{-1}. The *E. coli* polar lipid extract headgroup composition consisted of 67% phosphatidylethanolamine (PE), 23.2% phosphatidylglycerol (PG), and 9.8% cardiolipin (CL), with acyl chains reflecting the intrinsic composition of *E. coli* [45].

A 20 µL aliquot of lipid solution was added to 1.8 ml of salt solution in both *cis* and *trans* compartments of the Teflon chamber, which was divided by a 15 µm thick Teflon film with a *ca*. 200 µm diameter orifice suitable for bilayer formation (Fig. 5a). Given the lipophobic nature of the Teflon film, lipid adherence was enhanced by pre-treating the orifice with a 3% hexadecane solution in pentane, which imparts a more lipophilic surface. After pentane evaporation, the salt solution levels in both compartments were raised above the orifice, facilitating planar bilayer formation through monolayer apposition. Capacitance measurements confirmed appropriate bilayer formation. Two

distinct potassium chloride concentration gradients were employed for selectivity measurements: 250 mM KCl *cis* / 50 mM KCl *trans* (250/50 mM) and 50 mM KCl *cis* / 250 mM KCl *trans* (50/250 mM). For conductivity measurements, a symmetrical solution of 150 mM KCl *cis* / 150 mM KCl *trans* (150/150 mM) was used. All solutions were buffered with 5 mM HEPES at pH 7.4, with pH adjustment performed using a GLP22 pH meter (Crison). Tke5, dissolved in 20 mM Tris–HCl (pH 8), 150 mM NaCl, and 2 mM DTT, was added to the *cis* compartment to achieve a final concentration of 50 nM.

Ag/AgCl electrodes were custom-prepared within standard 250 µl pipette tips using 2 M KCl with 1.5% agarose bridges. A potential was considered positive when higher in the *cis* compartment (where the protein was always added), with the *trans* side set to ground. An Axopatch 200B amplifier (Molecular Devices, Sunnyvale, CA) in voltage-clamp mode facilitated current measurement and potential application. Collected data were filtered through an integrated 8-pole Bessel low-pass filter at 10 kHz and recorded with a sampling frequency of 50 kHz using a Digidata 1440A (Molecular Devices, Sunnyvale, CA). Data analysis was performed using pClamp 10 software (Molecular Devices, Sunnyvale, CA). For visualisation, current traces were digitally filtered with 500 Hz using a low-pass 8-pole Bessel filter.

The experimental setup, comprising a membrane chamber and head stage, was isolated from external noise sources by a double metal screen (Amuneal Manufacturing Corp., Philadelphia, PA). This configuration enabled measuring currents in the picoampere range with sub-millisecond time resolution. After potential application, the steady current was determined through Gaussian fitting of current value histograms. Currents were measured across a ± 0-100 mV range at 10 mV intervals, generating a single current-voltage (I-V) curve per experiment.

Ion selectivity measurements were conducted using concentration gradients between compartments of either 250/50 mM or 50/250 mM. Tke5-induced currents arise from the presence of at least one selective pore under a salt concentration gradient across compartments. The potential cation or anion preference of Tke5 currents was assessed by measuring the reversal potential (RP), defined as the applied voltage required to nullify the current.

A channel's ion selectivity is determined by the RP value: a non-zero RP indicates selective ion transport. For a cation-selective channel, the RP would be negative under the 250/50 mM gradient and positive under the 50/250 mM gradient, with the opposite pattern applying to an anion-selective channel. Obtained RP values, derived from linear regression of measured current-voltage (I-V) curves, were corrected for liquid junction potential using Henderson's equation to eliminate the salt bridge electrode contribution [46]. The corrected RP was subsequently introduced into the Goldman-Hodgkin-Katz (GHK) equation to calculate the channel permeability ratio (P^+/P^-) [47].

Channel conductance (G = I/V) was measured using a symmetric potassium chloride concentration of 150 mM/150 mM. Conductance increments (ΔG) were determined at ±100 mV, a voltage at which stable current increments or reductions were consistently observed. These ΔG values were calculated by averaging current increments (ΔI) and dividing by the applied voltage of ±100 mV. Normalised histograms of ΔG, generated with a 2.5 pS bin width, were fit to a single Gaussian distribution to determine the mean ΔG, which corresponded to the minimal channel conductance.

Plant pathogens growth inhibition assays

Vector pS238D•M or the derivate encoding the PelB-Tke5 effector (pS238D•*pelB-tke5*) (Table S2) were transferred to cells of phytopathogens *P. syringae, R. solanacearum, A. tumefaciens, D. dadantii, P. carotovorum, E. amylovora, X. campestris* and *P.*

savastanoi (Table S1) by conjugation as previously described. VBM agar supplemented with Km was used to select successfully transconjugants. The presence of the plasmids was corroborated by colony PCR using primers P4-P5 (Table S3). Overnight LB Lennox cultures of the abovementioned phytopathogens harbouring pS238D•M or pS238D•*pelB-tke5* were adjusted to an OD_{600} of 0.05 and 200 µL placed into a standard sterile 96 well-plate made of crystal-clear polystyrene with "U" form and 281 µL volume. The viability of the cells (OD_{600nm}) was measured every 15 minutes for 22 hours at 28ºC and 180 rpm using the Synergy/H1 microplate reader by Biotek©. Expression of *pelB-tke5* was induced after 2 hours with 0.5 mM of 3-*m*Bz except for *P. savastanoi* where 0.1 mM was used. 3-*m*Bz was also added to the strains harbouring the msfGFP expressing vector pS238D•M to control the intrinsic toxicity of 3-*m*Bz in the absence of the effector. Data was obtained from three biological replicates, each with technical duplicates.

Statistical analyses

Statistical analyses are based on Student's *t*-tests in which two conditions are compared independently. P-values from raw data were calculated by two-tailed t-test and from ratio data to the control by one-sample t-test using GraphPad Prism 8 version 8.3.0.

For flow cytometry assays, the Brown-Forsythe and Welch ANOVA Test with Dunnett's T3 multiple comparison test was performed to assess significant differences between the mean values of independent groups. Statistical significance was indicated as follows: not significant (ns), for $p > 0.05$, * for $p \leq 0.05$, ** for $p \leq 0.01$, *** for $p \leq 0.001$.

RESULTS

Tke5 is a putative T6SS-dependent effector

The first study to characterise the T6SSs in *P. putida* identified nine putative T6SS effectors (Tke1 to Tke9) in the KT2440 strain [21]. The study did not determine the function of any of these effectors; although some were predicted to be nucleases (Tke2 and Tke4) or colicins (Tke6 and Tke7), the function of others like Tke5 remained unknown [21]. Our current BLASTP analysis showed that Tke5 is a conserved T6SS component found in the Pseudomonadota phylum (formerly Proteobacteria), belonging to the BTH_I2691 family of the Conserved Domain Database (CDD), with accession number NF041559 (Fig. 1b). A phylogenetic tree using the reference proteins of this NCBI family shows a wide distribution within the Beta- and Gammaproteobacteria classes (Fig. 1a). Most β-proteobacteria were from the Burkholderiales order, while γ-proteobacteria were more diverse with many representatives from the Pseudomonadales order, but also Vibrionales and Enterobacteriales (Fig. 1a). BTH_I2691 protein family is the only member of the recently created superfamily cl49522 (October 2023). In *P. putida* Tke5 effector, the BTH_I2691 domain spans amino acids 10 to 858 from a total of 996 amino acids (*E*-value 1.33e-117; Fig. 1b) according to the BLASTP result. Additionally, the CDD revealed a MIX_II domain of the MIX superfamily, also known as the VasX_N superfamily in the Pfam database, which is included within the BTH_I2691 domain. This domain was first identified as a Marker for Type VI effectors [14] . Curiously, it was named VasX_N by the Pfam database because it was present in the N-terminal region of the T6SS element VasX from *V. cholerae*.

VasX is the only member of the family previously identified. It was first described as a virulence factor secreted by *V. cholerae* T6SS necessary to kill the host model system *Dictyostelium discoideum* [48,49]. Subsequently, VasX was shown to be also an

antimicrobial effector [49] which compromises the inner membrane of *Vibrio* species, and its activity is neutralised by the cognate immunity protein TsiV2 [48,49]. The effector presented a short domain (775-915 aa from 1085 aa) with homology to a pore-forming colicin also identified in Tke5 (Fig. 1b, dark blue) and preliminary results indicated that VasX compromised membrane integrity [50]. However, the exact mechanism of action of this effector is unknown.

The Conserved Domain Architecture Retrieval Tool (CDART) identified 61 different domain architectures within the BTH_I2691 protein family (Dataset S1) where the domain is found solo or in combination with many other domains. BTH_I2691 is mostly identified in the central part of these proteins (ranging from 1000 to 1500 amino acids) and interestingly, on many occasions, their N-terminal domains is also T6SS related. Fig. 1c shows representative proteins identified with CDART containing the T6SS-related domains *i.e.* MIX, PAAR, Tap (DUF4123), DUF2345 (VgrG related), LysM or even VgrG domains. Tke5 is most similar to Architecture number 2 which contains a BTH_I291 covering most of the protein and a single N-terminal MIX domain included in it (Fig. 1b).

To infer the function of this T6SS-related domain, we predicted the Tke5 topology that resulted in a 110-kDa membrane protein with five transmembrane domains (See Methods for details, Fig. 1d). Moreover, we predicted the putative structure of Tke5 using AlphaFold to perform a structural homology analysis with Foldseek [41]. This analysis retrieved that the Tke5 predicted structure was similar to the structure of *V. cholerae* toxin VasX from the AFDB Swissprot with an E-Value of 9.82e-22, and the highest probability value (1) (Fig. 1e), although the sequence identity was only 21% (Supplementary Fig. 1).

The genomic location of *tke5* within the K3-T6SS cluster (Fig. 2a), its structural homology to VasX, the presence of an N-terminal MIX domain associated with T6SS-dependent secretion, and a C-terminal colicin domain suggest that Tke5 may function as a T6SS-dependent toxin targeting the bacterial membrane.

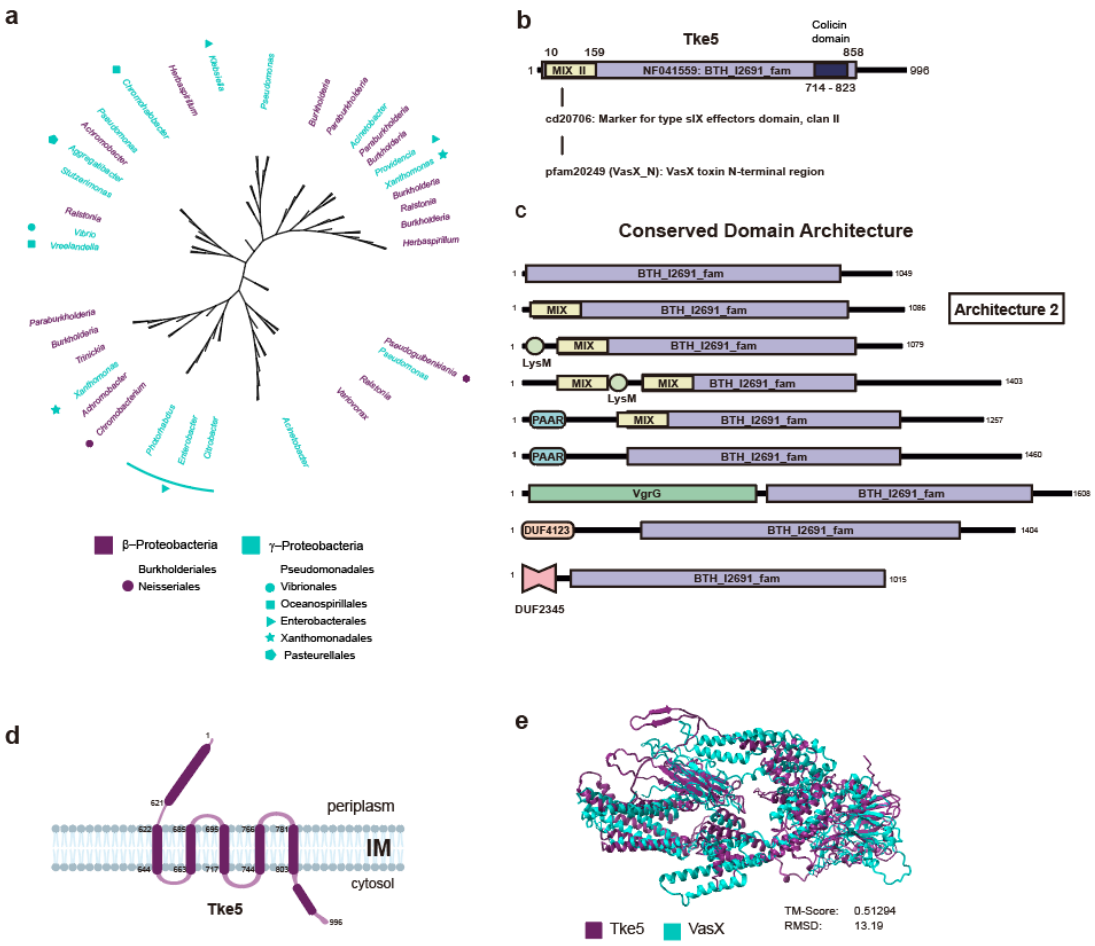

Figure 1 | Tke5 *in silico* study. **a)** Phylogenetic distribution of BTH_I2691 proteins in the Pseudomonadota phylum. A maximum likelihood tree with 500 bootstrap replicates was built with Mega 11 for the reference proteins of the BTH_I2691 family. **b)** Prediction of conserved domains in Tke5 using BLAST-P analysis, showing the spanned amino acids along with the corresponding reference names and identification numbers.

c) Conserved domain architecture of representative proteins within the BTH_I2691 family, indicating the amino acid spans and corresponding reference names. **d)** Topology prediction of Tke5 effector from *P. putida* T6SS. Tke5 transmembrane domain prediction was generated using TMHMM-2.0. **e)** Structural alignment of the AlphaFold Tke5 (purple) and VasX (cyan) models using Foldseek.

Tke5 is a potent antimicrobial toxin that can be neutralised by Tki5

To prove that Tke5 is an antimicrobial toxin, we tested the capacity of the putative Tke5 effector to impair bacterial growth when heterologously expressed from a plasmid. With this aim, the *tke5* gene was cloned into pS238D•M to produce pS238D•*tke5*. Additionally, a *pelB* sequence was fused to the *tke5* gene and cloned into pS238D•M to produce pS238D•*pelB-tke5*. The signal peptide PelB [51] was used to direct the effector to the Sec pathway to help a possible membrane insertion of Tke5 since the topology analysis revealed transmembrane helices, indicating that this effector might act within the bacterial membranes. The expression vector pS238D•M known as the digitaliser (ON/OFF) contains a complex regulatory circuit that allows having an OFF state of zero transcription in the absence of induction and thus is ideal for toxin expression [28]. The plasmids pS238D•*tke5* pS238D•*pelB-tke5* were transformed in *P. putida* KT2440 where the K3-T6SS is silenced.

The expression of the effector gene was induced after two hours of bacterial growth in LB Lennox by the addition of 3-*m*Bz. Upon induction of the putative effector, the growth of the tested strain was significantly impaired, especially when fused to PelB (dark purple curve, Fig. 2b) compared to the same strains harbouring the *msfGFP* reporter gene (light green curve, Fig. 2b). The expression of *msfGFP* was not

deleterious as expected for previous results from de Lorenzo's lab [28]. These data indicate that Tke5 is a potent antimicrobial toxin (Fig. 2b).

Importantly, bacteria with active T6SS require immunity proteins to prevent self-intoxication from their own T6SS antimicrobial effectors and to protect against friendly fire from sister cells. Immunity genes are frequently located downstream of their cognate toxin genes to secure co-expression and thus protection. Therefore, we asked if the gene downstream *tke5*, *i.e.*, *tki5*, codes for the immunity protein Tki5 (Fig. 2a). To assess the protective functionality of Tki5, the *tki5* gene was cloned into pSEVA624C, a vector compatible with pS238D (Fig. 2b) and then transformed in *P. putida* harbouring either pS238D•M, pS238D•*tke5* or pS238D•*pelB-tke5*. Expression of the immunity gene (*tki5*) was induced with IPTG at point zero, while the expression of the *tke5* toxin gene was induced with 3-*m*Bz two hours later. The co-expression of the putative *tki5* immunity gene together with the *tke5* or *pelB-tke5* rescued the impaired growth due to induction of the effector gene (light purple curves, Fig. 2b). Although Tki5 is predicted to insert into the cytoplasmic membrane (Fig. 2c), the expression of the *tki5* immunity gene in *P. putida* KT2440 does not exhibit toxicity (dark green curve, Fig. 2b), which is expected since KT2440 is the natural host of this protein. These data show that Tki5 protects *P. putida* KT2440 against Tke5 intoxication, demonstrating that Tke5/Tki5 are an effector-immunity (EI) pair.

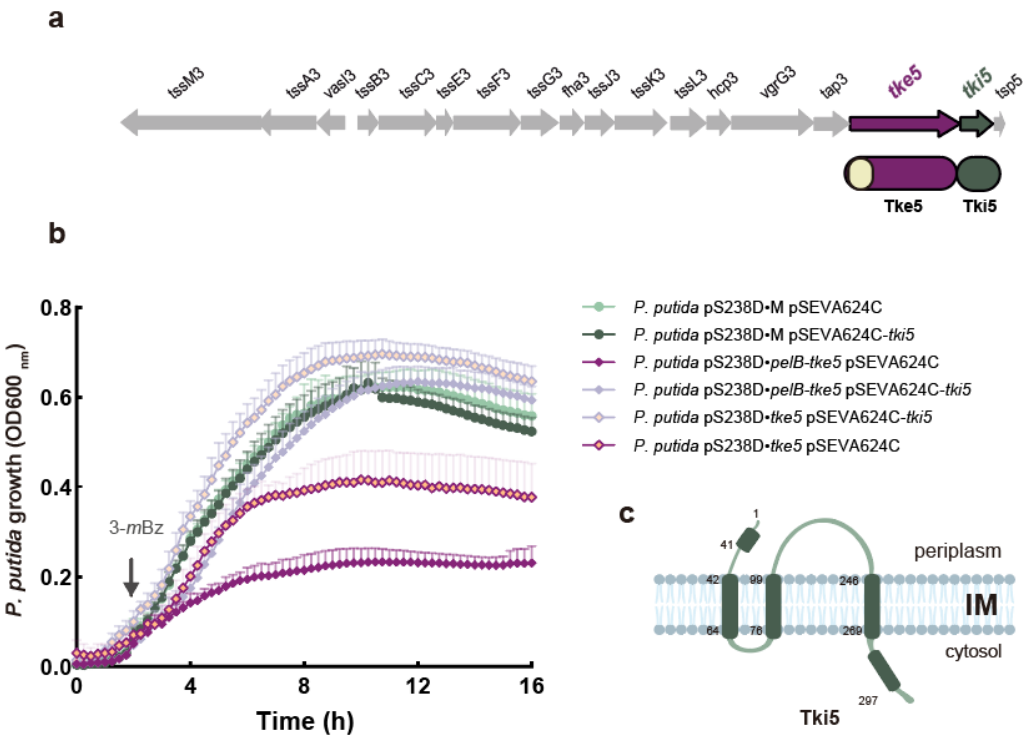

Figure 2 | Tke5 interaction with their cognate immunity pairs can protect *P. putida* KT2440 from self-toxicity. **a)** Schematic representation of the genomic organisation of the genes of the K3-T6SS cluster from *P. putida*. Genes encoding core and accessory components are shown in grey, the *tke5* effector gene is depicted in purple with the MIX domain in yellow and the *tki5* immunity gene is coloured in green. **b)** *P. putida* growth curves under Tke5-Tki5 EI pair production. Overnight cultures were adjusted to OD_{600} 0.1, and the immunity protein was immediately induced with 1 mM IPTG. After 2 h of initial incubation at 30ºC, effector expression (*tke5* or *pelB-tke5*) was induced by the addition of 0.5 mM 3-*m*Bz (indicated with an arrow). OD_{600} was measured for a total of 16 hours. **c)** Topology prediction of Tki5 immunity protein from *P. putida* T6SS. Tke5 transmembrane domain prediction was generated using TMHMM-2.0.

541

Tke5 is a bactericidal antimicrobial toxin

Here, we have demonstrated that Tke5 is a powerful antimicrobial toxin. Depending on their effect on bacterial targets, antimicrobial compounds can be classified as bactericidal if they kill bacteria, or bacteriostatic if they inhibit bacterial growth without directly killing the bacteria (*i.e.*, induce growth arrest). To determine whether Tke5 acts as a bactericidal or bacteriostatic agent, we performed cellular survival assays under expression of *tke5* using the laboratory host cell *E. coli* DH5α. Two antimicrobial substances with known mechanisms of action were used as controls: the bactericidal antibiotic gentamicin (Gm) and the bacteriostatic antibiotic tetracycline (Tc). Both target the 30S ribosomal subunit binding to the 16S rRNA, but their mechanisms differ significantly. Gm binds irreversibly, fooling the ribosome and leading to indiscriminate tRNAs acceptance which results in defective proteins and ultimately cell death. In contrast, Tc binds reversibly and prevents the peptide chain elongation. We have represented the cellular survival as the Log_{10} of the survival rate which is the ratio between the CFU at a given time and the CFU at time zero (Log_{10} survival rate [$CFU_{t=x}/CFU_{t=0}$]). Thus, the cellular survival of an organism growing in the absence of an antimicrobial compound will have a value greater than 0 (*E. coli* harbouring the empty plasmid in the absence of antimicrobial compound, light green curve, Fig. 3a). In the presence of a bacteriostatic agent, the CFU count remains constant over time, resulting in a survival rate of 1 and thus the Log_{10} representing cellular survival is 0 (*E. coli* harbouring the empty plasmid in the presence of Tc, dark green empty square curve, Fig. 3a). Conversely, a microorganism exposed to a bactericidal agent will present a cellular survival below 0 (*E. coli* harbouring the empty plasmid in the presence of Gm, dark green full square curve, Fig. 3a). Upon induction of *tke5*, *E. coli* survival at every tested point (hourly for a total of 6 hours) was consistently below 0 as a bactericidal

agent (dark purple diamond curve, Fig. 3a), while the uninduced strain (light purple diamond curve, Fig. 3a) reached a cellular survival above 2, showing growth similar to the strain with the empty plasmid.

Serial dilutions of these cultures were plated on LB agar plates at points 0, 3 and 6 hours to check survival (Fig. 3b). Individual CFU from cultures grown in the absence of antimicrobial compounds were visualised in the dilutions 10-e4 and 10-e5. As expected, the presence of Tc slightly decreased growth but did not kill the population while no CFU could be visualised in the cultures treated with Gm (Fig. 3b). Confirming the growth curve survival assay, the bactericidal effect of Tke5 was evident at 3 hours upon gene induction while the non-induced culture grew at the same level as the control strain (Fig. 3b). All this data indicates that Tke5 is a potent bactericidal toxin.

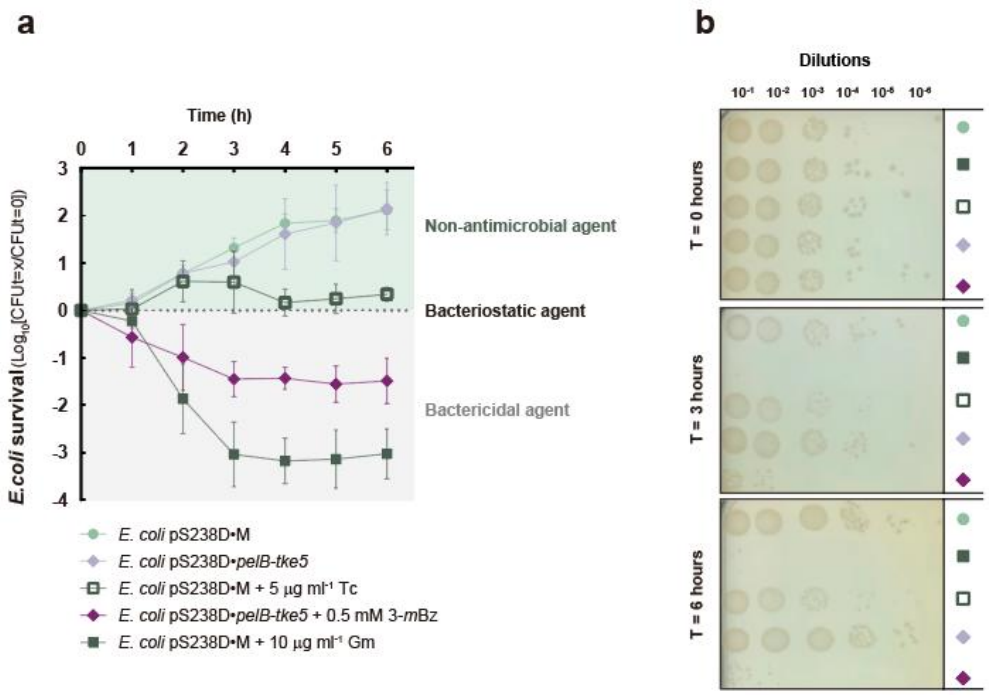

Figure 3 | Functionality of *P. putida* T6SS effector Tke5. **a)** Survival rate curve of *E. coli* DH5α upon induction of *tke5* expression. CFU survival was quantified over 6 h after induction with 0.5 mM 3-*m*Bz. Gentamicin and tetracycline were included for comparison. Bacteria

harbouring the *msfGFP*-bearing vector and the recombinant plasmid without induction were used as controls. 20 µL aliquots of each sample were taken hourly to determine the CFU ml^{-1} and calculate the Log_{10} survival rate ($CFU_{t=x}/CFU_{t=0}$). **b)** A subset (0, 3 and 6 hours) of each sample of *E. coli* DH5α cells from the different conditions tested in a) were plated in LB-agar to visualise the effect of Tke5 and the different controls on bacterial survival. The experiment was performed in triplicate.

578

579 ***Tke5 induces cell depolarization that can be neutralised by Tki5***

580 Our data support that Tke5 is a potent bactericidal toxin (Fig. 2b and 3) whose toxicity
581 is neutralised by the Tki5 immunity protein (Fig. 2b and 2c). Additionally, our
582 bioinformatic analysis suggested that Tke5 could be targeting the bacterial membrane
583 (Fig. 1d and 2c).

584 To evaluate this possibility, we measured the effect of Tke5 on cell permeability and
585 membrane potential of intoxicated *E. coli* DH5α cells using flow cytometry. To this end,
586 *E. coli* cells were transformed with the plasmid coding for Tke5 (pS238D•*tke5*) or the
587 variant encoding Tke5 fused to the PelB leader sequence (pS238D•*pelB-tke5*). Cells
588 were cultured in liquid media and the expression of *tke5* or *pelB-tke5* was induced with
589 3-*m*Bz. Two hours after *tke5* induction, cells were stained with Sytox™ Deep Red and
590 $DiBAC_4(3)$ to measure cell permeability and cell depolarisation, respectively. Sytox™
591 Deep Red is a nucleic acid stain that penetrates cells with compromised membranes
592 resulting in red fluorescence, thus allowing the detection of permeabilised cells by flow
593 cytometry [52]. $DiBAC_4(3)$ is an anionic probe that binds to intracellular proteins or the
594 membrane upon permeation into cells that have lost their resting membrane potential
595 and become depolarised, resulting in green fluorescence [53].

To define the possible cell populations resulting from the abovementioned treatment, *i.e.* healthy, permeabilised and depolarised cells, we performed the following controls: i) cell permeabilisation was induced by heat shock (red fluorescence, top left square, Supplementary Fig. 2a), ii) cell depolarisation was induced by treatment with polymyxin B antibiotic (green fluorescence, bottom right square, Supplementary Fig. 2b), and iii) untreated cells harbouring the empty pS238D plasmid uninduced and induced with 3-*m*Bz, represented the healthy population (mostly non-fluorescence, bottom left square, although *ca.* 7% showed green fluorescence, bottom right square, Supplementary Fig. 2c and 2d, respectively).

Measurements of cells expressing *tke5* and treated with Sytox™ Deep Red and DiBAC4(3) revealed that the production of Tke5 and PelB-Tke5 results in an approximate reduction of 5% and 16% in the healthy cell population, respectively, compared to the negative control (Fig. 4a, Supplementary Fig. 2e and f). These reductions in the healthy population corresponded with an increase in depolarised cells upon Tke5 and PelB-Tke5 induction (Fig. 4b, Supplementary Fig. 2e and f), while the percentage of permeabilised cells remained unchanged and near-zero (Fig. 4c, Supplementary Fig. 2e and f).

These results indicate that Tke5 and PelB-Tke5 alter the membrane potential of intoxicated cells without affecting the integrity of the cytoplasmic membrane. Consistent with our previous data (Fig. 2b), the impact of Tke5 is increased in the presence of the signal peptide PelB (Fig. 4b). As expected, based on results where Tke5 toxicity is neutralised by Tki5 (Fig. 2b), co-expression of PelB-Tke5 with the immunity protein Tki5 prevents cell depolarisation (see Methods for details; Fig. 4d-f and Supplementary Fig. 2g and h).

Given that our results suggest that Tke5 targets the cytoplasmic membrane of intoxicated cells, causing membrane depolarisation, we hypothesised that Tke5 may be a pore-forming protein that allows ion transport across the membrane, destabilising the resting membrane potential. This ion transport could represent the molecular mechanism employed by Tke5 to depolarise intoxicated cells.

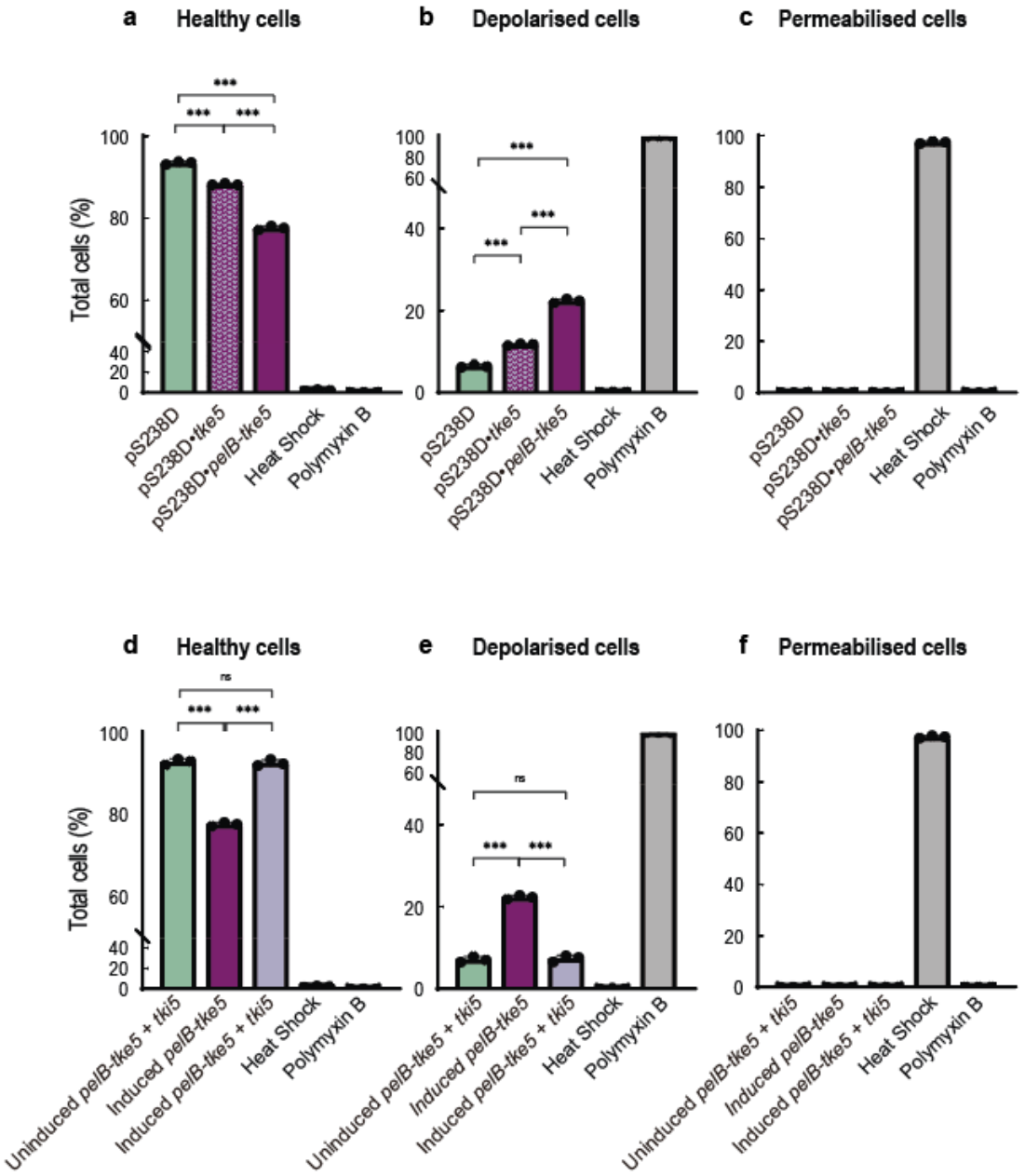

Figure 4 | Cell depolarisation induced by Tke5 effector and toxicity protection from

Tki5 immunity protein. Flow cytometry assays were carried out in *E. coli* DH5α cells transformed with the corresponding vectors and stained with both DiBAC4(3) (depolarised population) and Sytox™ Deep Red (permeabilised population). The upper row represents the percentage of healthy (**a**), depolarised (**b**) and permeabilised (**c**) cell populations upon production of Tke5 effector with and without being fused to PelB. Cells with the empty vector, subjected to heat shock and treated with polymyxin B are included as control samples. The bottom row represents the percentage of healthy (**d**), depolarised (**e**) and permeabilised (**f**) cell populations upon expression of PelB-Tke5 effector with and without the co-expression with the immunity protein Tki5. Cells without induction, subjected to heat shock and treated with polymyxin B are included as control samples.

Tke5 forms ion-selective pores in model membranes

To examine the ion channel activity of Tke5, we expressed and purified the protein from the cellular soluble fraction of *E. coli* BL21(DE3) cells co-transformed with pCOLADuet-1•*9xhis-tke5* and pSEVA624C•*tki5* plasmids (see Methods and Supplementary Fig. 3 for details) and evaluated its properties in a model membrane. Importantly, Tke5 is soluble in aqueous solution, exhibiting a dual state, either soluble or membrane-inserted, similar to pore-forming colicins. Using a modified solvent-free Montal-Mueller technique [44], we formed a synthetic lipid bilayer covering a small aperture separating two chambers (*cis* and *trans*) connected to an electric circuit (Fig. 5a). These chambers, filled with buffers of defined salt concentrations, provide a well-controlled artificial environment using only minimal amounts of material. In contrast to liposomes, one has direct access to both sides of the bilayer and therefore it is possible to work in asymmetric conditions in terms of electrolyte and membrane composition.

Following protein addition, we can measure ionic currents passing through Tke5-induced membrane pores. This experimental setup allows us to assess the pore conductance and ionic selectivity (cation *versus* anion preference).

To start, we assembled the synthetic lipid bilayer using an *E. coli* polar lipid extract in 150 mM KCl and confirmed membrane impermeability by ensuring the absence of leakage current. Then we added Tke5 to the *cis* chamber at a final concentration of 50 nM and waited for protein insertion until we observed stable currents indicative of ion flow through Tke5-formed pores. Fig. 5b shows a representative current trace (current intensities denoted as I) as a function of applied potential (V). The I/V relationship was linear at low voltages, indicating ohmic behaviour (Fig. 5c), while high voltages produced small stepwise current jumps (inset in Fig. 5b). Of note, the frequency of these random transitions between conducting levels increased when the voltage surpassed *ca.* 70 mV, indicating either a change in the number of Tke5 pores inserted into the lipid bilayer or, alternatively, dynamic structural changes in the pore size of already existing Tke5 channels.

To distinguish between these two possibilities, we first estimated the size of the Tke5 pore lumen, by measuring current jumps (ΔI) at a constant ±100 mV, and analysing the respective Tke5-pore conductance (ΔG), which reflects its current-carrying capacity, and the frequency of these occurrences across experiments. Histograms in Fig. 5d show a clear peak centred around G = 33 ± 4 pS, which aligns with the known conductance for gramicidin A, a channel-forming peptide with a well-established pore radius of ~0.4 nm in similar salt and lipid conditions [54–56]. Such a subnanometric pore diameter is typical of highly specialized narrow channels allowing only the transport of partially dehydrated ions while excluding larger hydrated ions, other solutes and metabolites [57].

The broad conductance range (10-80 pS) observed in Fig. 5d, may reflect some variability in the size of Tke5 pores formed among experiments or also the presence of multiple simultaneous insertions operating as clusters. To address this issue, we assessed the ionic selectivity of Tke5-induced pores by measuring the reversal potential (RP) and compared it with the conductance data. The RP is the potential needed to null the current flow through the channel under asymmetric salt conditions [58,59]. Since the physical dimensions of the channel lumen define the intensity of the interaction between the pore charges and the permeating ions, the ionic selectivity of the channel increases as the channel becomes narrower, and vice versa. Accordingly, if the RP necessary to counteract the flow of ions does not change significantly with G, this would mean that a number of quasi-identical channels are inserted simultaneously in the membrane. In contrast, a decrease in RP with increasing G would indicate a size-dependent population of channels [59,60].

To study the RP of Tke5 channels, we measured induced currents at two concentration gradients: first with 250 mM KCl in the *cis* chamber and 50 mM KCl in the *trans* chamber (250/50 mM KCl), and then with an inverted gradient of 50/250 mM KCl, (dark blue/light blue data represented in Fig. 5e-h). The gradient mimics the ion concentration differences across bacterial membranes, where total ion concentrations are higher in the periplasm than in the cytosol as a result of charged macromolecules being unable to cross the inner membrane. Representative current traces with the 250/50 mM and 50/250 mM KCl gradients are shown in Fig. 5e. For each experimental trace, we plotted the I/V curve (Fig. 5f) to confirm the ohmic behaviour and calculated the conductance associated with each RP measurement (Fig. 5g). In the 250/50 mM KCl gradient, the Tke5 currents produced values of RP ~ 30 mV which is similar to the absolute RP obtained in the 50/250 mM KCl gradient ~ -30. The fact that RP does not

change significantly in a variety of Tke5 channels displaying different G values (several orders of magnitude) suggests the presence of clusters of channels with similar dimensions adding to the total ion flow rather than the assembly of larger pores, which would have altered considerably the RP values in Fig. 5g.

The RP also reveals channel selectivity, *i.e.* its relative preference for cations *versus* anions. When a channel favours cations, more positive ions move through the channel from the side with a higher concentration to the side with a lower concentration. Therefore, when the salt concentration is higher on the *cis* side and lower on the *trans* side (250/50 mM KCl gradient), the RP will be negative to counteract the movement of the cations from *cis* to *trans* chambers (note that in our set up the *trans* compartment is grounded, see Methods). Conversely, if the gradient is inverted, the RP will be positive. This is exactly what we observed in our setup where the average RP for the 250/50 mM KCl gradient is negative (-31±2 mV), while the average RP for the 50/250 mM KCl gradient is positive (+33±3 mV) (Fig. 5g), indicating that Tke5 channels preferentially allow positively charged ions (such as K^+) to flow through.

Lastly, to obtain a quantitative estimation of the ratio between the flow of cations and anions, *i.e.* the ion permeability ratio (P_{K^+}/P_{Cl^-}), we used the Goldman-Hodgkin-Katz flux equation (GHK, [61]), which yielded values of P_{K^+}/P_{Cl^-} = 10 ± 3 and 16 ±9 in the 250/50 and 50/250 mM KCl gradient, respectively (Fig. 5h), (note that GHK equation shows an exponential relationship between P_{K^+}/P_{Cl^-} and RP, so that small changes in RP yield noticeable differences in P_{K^+}/P_{Cl^-}). Weakly selective channels tend to have a P_{K^+}/P_{Cl^-} <5, while ideal selective channels can reach values of 100-1000 [57,59]. Therefore, these results indicate that Tke5 forms ionic channels ~0.8 nm in diameter with a relatively high preference for K^+ over Cl^- ions.

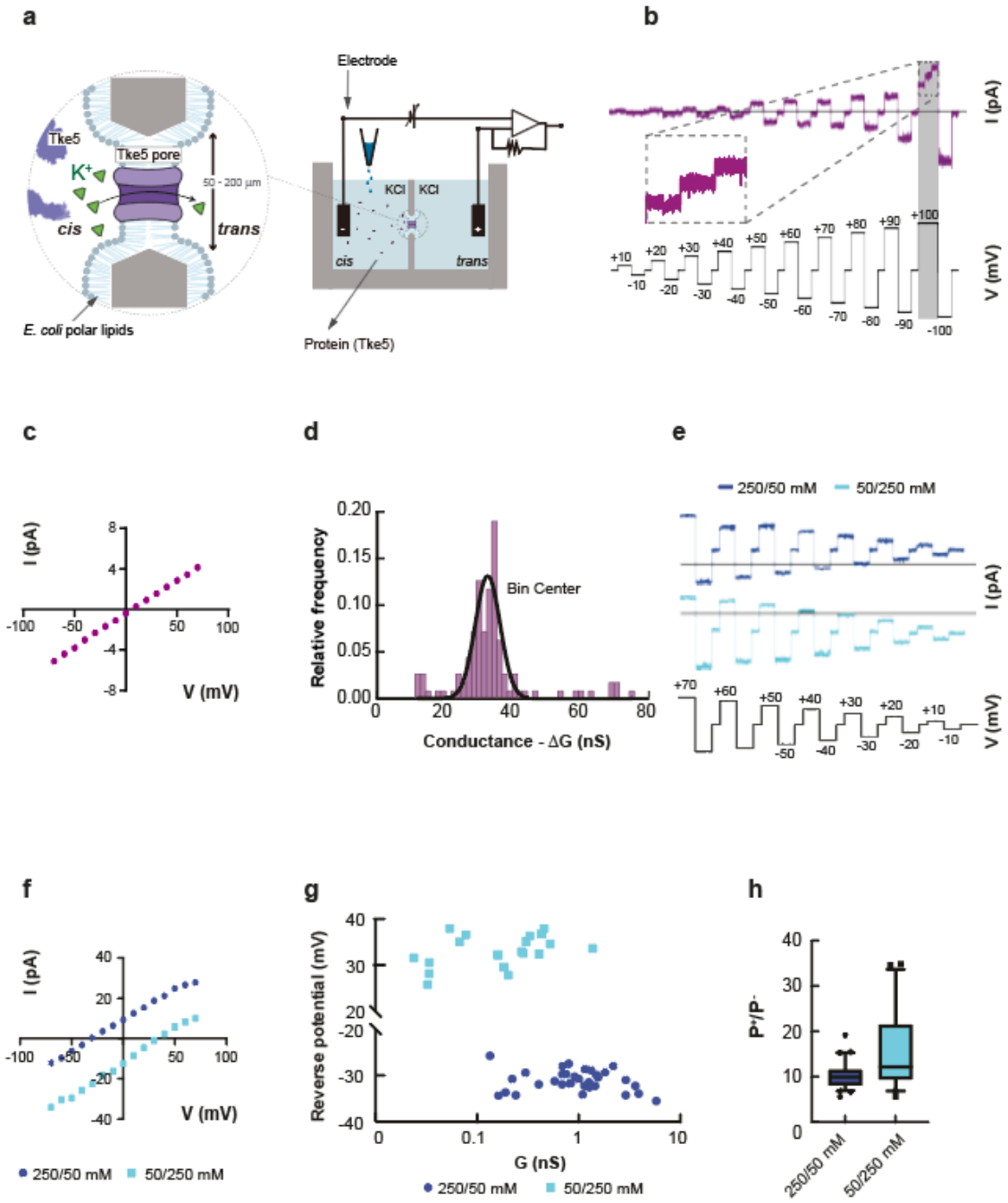

Figure 5 | Tke5 forms stable, cation-selective pores in model membranes. **a)** Schematic of a Montal-Mueller setup to form a synthetic membrane from an *E. coli* polar lipid extract. **b)** Representative stable current trace induced by Tke5 under symmetric 150/150 mM KCl condition. The horizontal black line marks zero current, with applied voltages labelled below. A grey rectangle highlights current increments at +100 mV voltage. **c)** Current-voltage (I/V) plot corresponding to the trace in (b). **d**) Normalised histogram (bin of 2.5) showing conductance increments (ΔG = ΔI / V) at ± 100 mV in

150/150 mM KCl. Values are fitted to a Gaussian, with the mean ΔG representing the minimal channel conductance jumps. **e)** Representative stable current traces induced by Tke5 in asymmetric 250/50 mM and 50/250 mM KCl conditions, shown in dark and light blue, respectively. The horizontal black line indicates zero current, and applied voltages are marked below. **f)** I/V plots for traces in (e). **g)** Plot of RP (mV) versus conductance (nS) for independent measurements in 250/50 mM and 50/250 mM KCl conditions. A negative RP in 250/50 mM KCl gradient condition and a positive RP value in the 50/250 mM KCl gradient condition indicate Tke5 cation selectivity. **h)** Box plot showing cation/anion permeability ratios (P^+/P^-) derived from RP values in (**g**), calculated using the GHK equation that considers the gradient. Boxes display the 25th and 75th percentiles, with median lines inside and whiskers indicating standard deviation.

The Tke5 toxin kills plant pathogens

P. putida is a biocontrol agent that uses the T6SS to kill plant pathogens *i.e.* phytopathogens [21]. Thus, we tested the capacity of the putative Tke5 effector to kill phytopathogens of importance for agriculture. We selected a list of pathogens that included at least one strain of most of the Top 10 plant pathogenic bacteria species based on scientific and economic importance [62] *i.e.*, (1) *Pseudomonas syringae* pathovars; (2) *Ralstonia solanacearum*; (3) *Agrobacterium tumefaciens*; (4) *Xanthomonas oryzae*; (5) *Xanthomonas campestris*; (6) *Xanthomonas axonopodis*; (7) *Erwinia amylovora*; (8) *Xylella fastidiosa*; (9) *Dickeya dadantii*; (10) *Pectobacterium carotovorum*, and *Pseudomonas savastanoi* just missing the podium.

Among the crops affected by these phytopathogens are brassica crops including broccoli, cauliflower, cabbage, turnip, and mustard (*X. campestris*); coffee, kiwi,

726 tomato, rice, beans, cherry, plum, horse chestnut, loquat (*P. syringae*); carrot, potato,
727 leafy greens, squash, onion, peppers (*P. carotovorum*); walnuts, grapevines, stone fruits,
728 nut trees, sugar beets, horseradish, rhubarb (*A. tumefaciens*) and olive trees, oleander,
729 and ash trees (*P. savastanoi*); the main causal agents are indicated in brackets
730 immediately after the affected crops.

731 To test the efficiency of Tke5 in impairing the growth of plant pathogens, the broad-host
732 range plasmid pS238D•*pelB-tke5* was transferred by conjugation to the strains of
733 interest *i.e.*, *P. syringae* pv. syringae B728a, *R. solanacearum* NCPPB 1493, *A.*
734 *tumefaciens* C58, *D. dadantii* 3937, *P. carotovorum* subsp. carotovorum SCRI 194, *E.*
735 *amylovora* NCPPB 595, *X. campestris* pv vesicatoria NCPPB 195 and *P. savastanoi* pv.
736 savastanoi NCPPB 3335. The expression of the effector gene was induced after two
737 hours of bacterial growth in LB Lennox by the addition of 3-*m*Bz. Upon induction of
738 the putative effector, the growth of the different tested plant pathogens was significantly
739 impaired in all cases (dark purple curve, Fig. 6) compared to their controls, that is, the
740 same strains harbouring the pS238D•M vector (green curves, Fig. 6) or without 3-*m*Bz
741 induction (light purple curve, Fig. 6). The addition of 3-*m*Bz to the plant pathogen
742 strains harbouring the pS238D•M vector, which expresses the *msfGFP* reporter gene
743 instead of the *tke5* gene effector, demonstrated that: i) the concentration of 3-*m*Bz used
744 in our assay is not toxic to these strains, and ii) the level of expression of this system is
745 not inherently toxic, as the production of a non-toxic protein, msfGFP, did not affect the
746 survival of these strains (dark green curve, Fig. 6).

747 All these data demonstrate the potent antibacterial activity of the Tke5 T6SS toxin
748 against a diverse range of economically significant plant pathogens. The broad-
749 spectrum inhibitory effect suggests that Tke5 could be a valuable molecular tool for
750 enhancing the biocontrol capabilities of *P. putida* in agricultural settings. By targeting

multiple phytopathogens that threaten crops across various agricultural ecosystems, Tke5 represents a promising strategy for developing more effective and targeted biological control mechanisms.

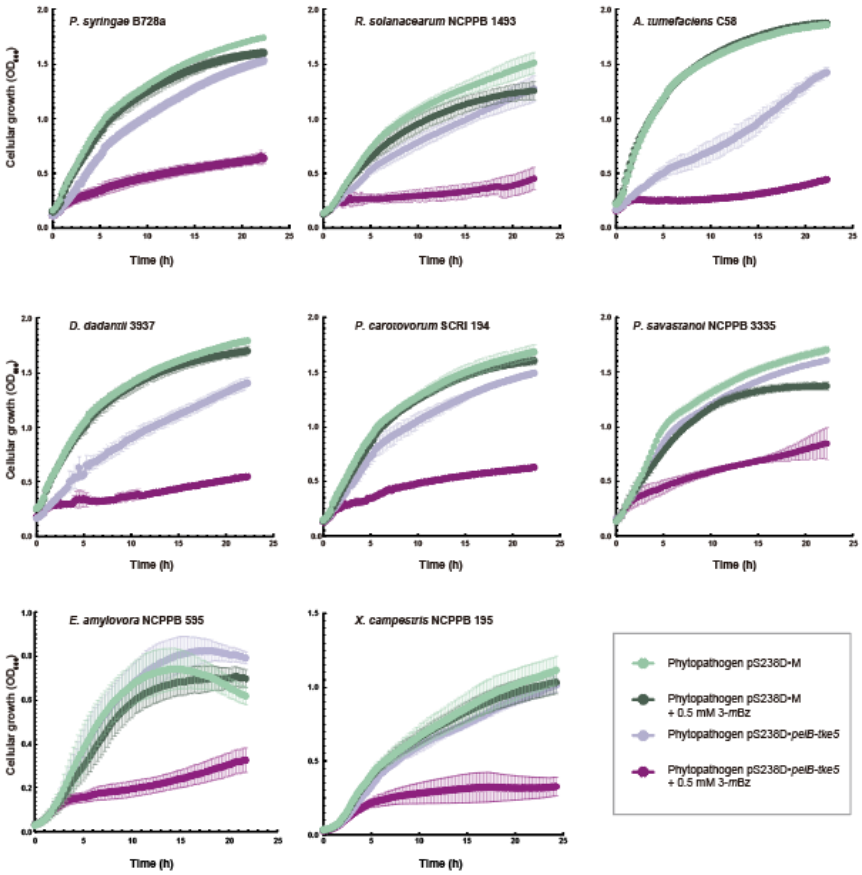

Figure 6 | Toxicity of Tke5 for different recalcitrant phytopathogens. The growth of plant pathogens cells harbouring the pS238D•*pelB-tke5* containing the T6SS effector of *P. putida* Tke5 N-terminal fused to a PelB signal peptide was determined by measuring the OD at 600 nm every 15 minutes for 22 hours at 28ºC using the Synergy/H1 microplate reader by Biotek©. After 2 hours, 3-*m*Bz was added to the LB medium to induce the expression of the *pelB-tke5* gene.

DISCUSSION

The identification and characterisation of novel protein toxins increase our molecular-level understanding of bacterial competition and the dynamics of microbial communities. This can be especially relevant in complex environments like the rhizosphere (surrounding plant roots) and phyllosphere (surrounding plant leaves) where rival bacteria compete to colonise plants. Biocontrol agents in these complex environments, like *P. putida*, use the T6SS as a potent system to eliminate harmful phytopathogen competitors and protect crops from their infections. Here we describe Tke5, a novel potent protein toxin produced by *P. putida* with killing capabilities against the current most recalcitrant phytopathogens.

Tke5 is encoded within the K3-T6SS cluster and our bioinformatic analysis suggests it is a conserved T6SS component within the Pseudomonadota phylum (Fig. 1a-c). Tke5 represents the first member of the BTH_I2691 family to be studied at the molecular level. Another member of this family, VasX, was shown to be a *V. cholerae* T6SS-dependent virulence factor crucial to killing *Dictyostelium discoideum* [48] and later studies revealed it also functions as an antimicrobial effector, targeting the inner membrane of other *Vibrio* species leading to depolarisation and subsequent bacterial death [50]. Structural predictions of Tke5 suggest the presence of a MIX_II N-terminal (Fig. 1b), a well-established marker of T6SS effectors [14], which is also predicted in VasX. Additionally, Tke5 is predicted to contain multiple transmembrane domains (Fig. 1d), a characteristic also present in VasX, which is associated with its membrane-targeting activity [50].

In the present study, we show that Tke5 exhibits potent antibacterial activity in growth inhibition assays using *P. putida* (Fig. 2). The effector is not merely bacteriostatic but actively kills target bacteria mirroring the effects of a bactericidal antibiotic (Fig. 3)

without provoking cellular lysis. Flow cytometry data indicates that the bactericidal effect is due to cell depolarisation which occurs without compromising cell permeability, suggesting that Tke5 permeabilise the inner membrane of the bacteria, but maintains membrane integrity (Fig. 4).

To shade some light into the molecular mechanism underlying its cell depolarisation activity, we exploit electrophysiology using an *in vitro* model membrane (Fig. 5a). The observation of stable currents across the synthetic lipid bilayer upon Tke5 addition provides strong evidence for the formation of ion-selective pores (Fig. 5b-c). Further analysis of the RP under asymmetric salt concentrations (250/50 and 50/250 mM KCl in the cis/trans chambers) reveals that Tke5-induced pores allow the passive multiionic transport of ions, but with some preference for cations (K^+) over anions (Cl^-), as indicated by a calculated ion permeability ratio (P_+/P_-) ≈ 10. Furthermore, the RP is constant between traces of varying conductance levels (RP = –31 ±2 mV or +33 ±3 mV in a 250/50 or a 50/250 mM KCl gradient, respectively), which indicates Tke5 assembles a varying number of pores in each experimental replicate, but the structural characteristic of each pore is highly similar (Fig. 5e-g).

The capacity of Tke5 to permeate ions across the lipid bilayer is consistent with its cell depolarisation activity. Thus, we would expect that *in vivo*, Tke5 passively transports ions, with some preference for cations, from outside the cell, where they are found at higher concentrations, to inside the cell. This transport disrupts the delicate balance of ions across the membrane, which is crucial for maintaining ionic homeostasis and is essential for preserving the membrane potential and all the cellular processes that depend on it.

Several T6SS effectors have been identified that form ion-selective pores in the membranes of target cells, disrupting the membrane potential of the target cell and leading to cell death. The C-terminal fragment of Tse5 (Tse5-CT) from *P. aeruginosa* is a PFT that was postulated to assemble proteolipidic pores in the inner membrane of Gram-negative bacteria [5]. In this case, an ion permeability ratio value less than 6 in a 250/50 KCl gradient ($P_+/P_- \leq 6$) was measured using a model membrane with the same lipid composition (the *E. coli* polar lipid extract). Another example is Ssp6, found in *Serratia marcescens*, an antibacterial effector that mainly causes cell depolarisation [63]. For Ssp6, a RP = –26.5 mV was obtained in artificial membranes and non-symmetrical KCl conditions (510/210 mM KCl in *cis* and *trans* chambers, respectively).

Recently, a novel family of contact-dependent inhibition (CDI) effectors has been studied in *E. coli* [64].This new family causes cell depolarisation, while minimal cell permeability was detected. Competition experiments demonstrate that these toxins are highly effective, with ~82% of target cells showing depolarisation in representative assays. However, propidium iodide (PI) uptake, indicating loss of membrane integrity, was observed in only a minor fraction of cells. These results suggest these effectors might also be ionophoric protein toxins that assemble ion-selective membrane pores, causing cell depolarisation.

Unlike Tke5 and VasX, which are large proteins with approximately 1,000 amino acids, Tse5-CT, Ssp6, and the C-terminal fragments of CDI toxins represent a contrasting group of small toxins between ~150-230 amino-acid residues. Despite significant differences in size, sequence, and origin, these toxins appear to converge on a similar mode of action, preferentially inserting into the inner membrane of intoxicated bacteria. This shared functional outcome underscores a fascinating case of convergent evolution

in toxin mechanisms, likely driven by the same selective pressures to efficiently disrupt bacterial competitors.

Tke5, likely employs its N-terminal MIX domain for T6SS-dependent delivery into the target cell, while its C-terminal colicin-like domain is probably involved in causing cell depolarization through ion channel formation. Our experimental data using synthetic lipid bilayers demonstrate that Tke5 forms stable, ion-selective pores with multi-ionic character and some preference for cations like K^+, presumably destabilizing the resting membrane potential of target bacteria. Notably, the measured ion conductance reveals that Tke5 inserts more efficiently under a 250/50 mM salt gradient, where the *cis* side of the bilayer, representing the periplasm, is more shielded than the *trans* side, which mimics the cytoplasm. This setup generates a negative membrane potential simulating physiological conditions, supporting the hypothesis that Tke5 inserts preferentially from the periplasm. Moreover, in vivo data show that Tke5 exhibits greater toxicity when directed to the Sec pathway compared to cytoplasmic expression (Fig. 2b), further supporting the periplasmic insertion model. A similar effect has been seen for Tse5, which senses the directionality of the membrane potential, and can only release its encapsulated Tse5-CT fragment when introduced in the *cis* chamber under a 250/50 mM salt gradient, and not under a 50/250 mM salt gradient [5]. An even more dramatic effect is seen with Ssp6 from *Serratia*, which is not toxic when overproduced in the cytosol of *E. coli* and only forms ion channels when directed to the Sec translocon or delivered by the T6SS in a competition assay [63].

Tki5 expression protects *P. putida* from Tke5 toxicity (Fig. 2, 3), confirming that Tke5/Tki5 functions as a genuine E/I pair. Tki5 is predicted to be a transmembrane protein, which suggests it likely interacts with Tke5 at the membrane level to protect *P. putida* from self-intoxication and attack by sibling cells. A similar effect has been shown

for VasX and its immunity protein TsiV2 [50]. However, the precise mechanism of this interaction remains to be elucidated.

In this study, we also highlight the ecological relevance of Tke5 by demonstrating its potent antibacterial activity against various plant pathogens. Expression of *tke5* significantly impaired growth in multiple phytopathogens including *P. syringae, R. solanacearum, A. tumefaciens, D. dadantii, P. carotovorum, E. amylovora, X. campestris,* and *P. savastanoi* compared to controls (Fig. 6). Control strains carrying empty vector or expressing non-toxic *msfGFP* grew normally with inducer (3-*m*Bz), confirming that growth inhibition stems directly from Tke5 activity. By effectively targeting and neutralising these economically important plant pathogens, Tke5 could play a crucial role in protecting crops and ensuring agricultural productivity. This would add a novel weapon to the *P. putida* arsenal after the already known effector secreted by the K1-T6SS such as the Tke2 nuclease [21] and the Tke7 colicin.

While T6SS is common in plant-associated bacteria [65], only a few T6SS effectors with biocontrol activity have been characterised. One example is the T6SS amidase Tae3^{Pf} from *P. fluorescens* MFE01, which protects against *Pectobacterium atrosepticum* [66]. Several beneficial bacteria employ T6SS for plant colonization and pathogen defence, though their specific effectors remain uncharacterized. For instance, *A. brasilense* T6SS clusters provide antibacterial activity against multiple plant pathogens [67]. Similarly, *P. chlororaphis* uses T6SSs to compete against pathogens like *A. tumefaciens* C58 and *P. syringae* pv. tomato DC3000 [68]. The F1- and F3-T6SS in *P. fluorescens* F113 are crucial for rhizosphere persistence, as demonstrated by the reduced fitness of T6SS-deficient mutants [69]. In *P. fluorescens* Pf29Arp, T6SS genes show differential expression between healthy and pathogen-infected wheat roots, suggesting adaptation roles [70]. Even plant pathogens like *A. citrulli* seems to use T6SS to inhibit other pathogens, reducing rice

bacterial blight symptoms caused by *X. oryzae* pv. oryzae [71]. In symbiotic bacteria, T6SS enhances host colonization, as seen in the improved competitiveness of *Sinorhizobium freddii* in *G. max* cv Pekin nodules [72].

The characterisation of Tke5 as a novel, pore-forming, bactericidal toxin effector expands our understanding of the sophisticated weaponry employed by bacteria in interbacterial competition. Its activity against plant pathogens further suggests a key role in shaping microbial communities and influencing plant health. This knowledge can inform the development of novel biocontrol strategies and contribute to the ongoing efforts to reduce dependence on chemical pesticides.

ACKNOWLEDGEMENTS

P.B. acknowledges the financial support received from the Spanish Minister of Science, Innovation and Universities (MICIU/AEI/10.13039/501100011033) through the *Ramón y Cajal* Program (RYC2019-026551-I, ESF Investing in your future), the research grant from the State Subprogram for Knowledge Generation PID2021-123000OB-I00 (ERDF/EU) and the research grant from the State Subprogram for Promotion of Research Consolidation CNS2022-135585 (European Union NextGenerationEU/PRTR).

D.A.-J. acknowledges support by the MICIU Contract PID2021-127816NB-I00 and the Basque Government's Department of Education IT1745-22.

A.A. and M.Q.-M. acknowledge financial support by the Spanish Government MICIU/AEI/10.13039/501100011033/FEDER, UE (Project 2019-108434GB-I00 and Project PID2022-142795 NB-I00), Generalitat Valenciana (project CIGRIS/2021/021) and Universitat Jaume I (Project UJI-B2022-42). M.Q.-M acknowledges support from

the Spanish Ministry of Science and Innovation (Project IJC2018-035283-I funded by MICIU/AEI/10.13039/501100011033) and Universitat Jaume I (project UJI-A2020-21).

We thank Cayo Ramos, Emilia López Solanilla, Francisco M. Cazorla, Ehr Min Lai, María Milagros López and Inmaculada Sampedro for their kind gifts of phytopathogenic strains.

CONFLICTS OF INTEREST STATEMENT

The authors declare no conflict of interest.

DATA AVAILABILITY STATEMENT

The data are available within the manuscript. The sequence of a newly generated vector available as a tool for the scientific community has been deposited into NCBI Genbank with accession number PQ628036 and into the SEVA repository https://seva-plasmids.com/.

REFERENCES

1. Mondal, A. K., Verma, P., Lata, K., Singh, M., Chatterjee, S. & Chattopadhyay, K. Sequence Diversity in the Pore-Forming Motifs of the Membrane-Damaging Protein Toxins. *Journal of Membrane Biology* **253,** 469–478 Preprint at https://doi.org/10.1007/s00232-020-00141-2 (2020)

2. Carruthers, V. B. Apicomplexan Pore-Forming Toxins. *Annu Rev Microbiol* **78,** 277–291 (2024).

3. Peraro, M. D. & Van Der Goot, F. G. Pore-forming toxins: Ancient, but never really out of fashion. *Nat Rev Microbiol* **14,** 77–92 Preprint at https://doi.org/10.1038/nrmicro.2015.3 (2016)

4. González-Magaña, A., Altuna, J., Queralt-Martín, M., Largo, E., Velázquez, C., Montánchez, I., Bernal, P., Alcaraz, A. & Albesa-Jové, D. The *P. aeruginosa* effector Tse5 forms membrane pores disrupting the membrane potential of intoxicated bacteria. *Commun Biol* **5,** 1189 (2022).

930 5. González-Magaña, A., Tascón, I., Altuna-Alvarez, J., Queralt-Martín, M., Colautti, J.,
931 Velázquez, C., Zabala, M., Rojas-Palomino, J., Cárdenas, M., Alcaraz, A., Whitney, J.
932 C., Ubarretxena-Belandia, I. & Albesa-Jové, D. Structural and functional insights
933 into the delivery of a bacterial Rhs pore-forming toxin to the membrane. *Nat*
934 *Commun* **14,** 7808 (2023).

935 6. Allsopp, L. P. & Bernal, P. Killing in the name of: T6SS structure and effector
936 diversity. *Microbiology (N Y)* **169,** 1367 (2023).

937 7. Rapisarda, C., Cherrak, Y., Kooger, R., Schmidt, V., Pellarin, R., Logger, L., Cascales,
938 E., Pilhofer, M., Durand, E. & Fronzes, R. In situ and high-resolution cryo-EM
939 structure of a bacterial type VI secretion system membrane complex. *EMBO J* **38,**
940 e100886 (2019).

941 8. Cherrak, Y., Rapisarda, C., Pellarin, R., Bouvier, G., Bardiaux, B., Allain, F., Malosse,
942 C., Rey, M., Chamot-Rooke, J., Cascales, E., Fronzes, R. & Durand, E. Biogenesis and
943 structure of a type VI secretion baseplate. *Nat Microbiol* **3,** 1404–1416 (2018).

944 9. Zoued, A., Durand, E., Brunet, Y. R., Spinelli, S., Douzi, B., Guzzo, M., Flaugnatti, N.,
945 Legrand, P., Journet, L., Fronzes, R., Mignot, T., Cambillau, C. & Cascales, E. Priming
946 and polymerization of a bacterial contractile tail structure. *Nature* **531,** 59–63
947 (2016).

948 10. Kudryashev, M., Wang, R. Y. R., Brackmann, M., Scherer, S., Maier, T., Baker, D.,
949 Dimaio, F., Stahlberg, H., Egelman, E. H. & Basler, M. Structure of the Type VI
950 secretion system contractile sheath. *Cell* **160,** 952–962 (2015).

951 11. Basler, M., Pilhofer, M., Henderson, G. P., Jensen, G. J. & Mekalanos, J. J. Type VI
952 secretion requires a dynamic contractile phage tail-like structure. *Nature* **483,**
953 182–186 (2012).

954 12. Bernal, P., Furniss, R. C. D., Fecht, S., Leung, R. C. Y., Spiga, L., Mavridou, D. A. I. &
955 Filloux, A. A novel stabilization mechanism for the type VI secretion system sheath.
956 *Proc Natl Acad Sci U S A* **118,** e2008500118 (2021).

957 13. Santin, Y. G., Doan, T., Lebrun, R., Espinosa, L., Journet, L. & Cascales, E. In vivo
958 TssA proximity labelling during type VI secretion biogenesis reveals TagA as a
959 protein that stops and holds the sheath. *Nat Microbiol* **3,** 1304–1313 (2018).

960 14. Salomon, D., Kinch, L. N., Trudgian, D. C., Guo, X., Klimko, J. A., Grishin, N. V.,
961 Mirzaei, H. & Orth, K. Marker for type VI secretion system effectors. *Proc Natl Acad*
962 *Sci U S A* **111,** 9271–9276 (2014).

963 15. Bernal, P. T6SS-effector hunters uncover PIX: a novel delivery/marker domain.
964 *Trends Microbiol* **32,** 617–619 (2024).

965 16. Kanarek, K., Fridman, C. M., Bosis, E. & Salomon, D. The RIX domain defines a class
966 of polymorphic T6SS effectors and secreted adaptors. *Nat Commun* **14,** 4983
967 (2023).

968 17. Jana, B., Fridman, C. M., Bosis, E. & Salomon, D. A modular effector with a DNase
969 domain and a marker for T6SS substrates. *Nat Commun* **10,** 3595 (2019).

970 18. Carobbi, A., Leo, K., Di Nepi, S., Bosis, E., Salomon, D. & Sessa, G. PIX is an N-
971 terminal delivery domain that defines a class of polymorphic T6SS effectors in
972 *Enterobacterales*. *Cell Rep* **43,** 114015 (2024).

973 19. Ruhe, Z. C., Low, D. A. & Hayes, C. S. Polymorphic Toxins and Their Immunity
974 Proteins: Diversity, Evolution, and Mechanisms of Delivery. *Annu Rev Microbiol* **74,**
975 497–520 (2020).

976 20. Weller, D. M. *Pseudomonas* Biocontrol Agents of Soilborne Pathogens: Looking
977 Back Over 30 Years. *Phytopathology* **97,** 250–256 (2007).

978 21. Bernal, P., Allsopp, L. P., Filloux, A. & Llamas, M. A. The *Pseudomonas putida* T6SS
979 is a plant warden against phytopathogens. *ISME Journal* **11,** 972–987 (2017).

980 22. Bernal, P., Civantos, C., Pacheco-Sánchez, D., Quesada, J. M., Filloux, A. & Llamas,
981 M. A. Transcriptional organization and regulation of the *Pseudomonas putida* K1
982 type VI secretion system gene cluster. *Microbiology (N Y)* **169,** 001295 (2023).

983 23. Sambrook, J., Fritsch, E. F. & Maniatis, T. *Molecular Cloning: A Laboratory Manual.*
984 (Molecular Cloning: A Laboratory Manual, 1989).

985 24. Choi, K.-H., Kumar, A. & Schweizer, H. P. A 10-min method for preparation of highly
986 electrocompetent *Pseudomonas aeruginosa* cells: application for DNA fragment
987 transfer between chromosomes and plasmid transformation. *J Microbiol Methods*
988 **64,** 391–397 (2006).

989 25. Ramos-Gonzalez, M. I., Duque, E. & Ramos, J. L. Conjugational transfer of
990 recombinant DNA in cultures and in soils: host range of *Pseudomonas putida* TOL
991 plasmids. *Appl Environ Microbiol* **57,** 3020–3027 (1991).

992 26. Lei, S.-P., Lin, H.-C., Wang, S.-S., Callaway, J. & Wilcox, G. Characterization of the
993 *Erwinia carotovora pelB* Gene and Its Product Pectate Lyase. *J Bacteriol* **169,** 4379–
994 4383 (1987).

995 27. Tsirigotaki, A., De Geyter, J., Šoštarić, N., Economou, A. & Karamanou, S. Protein
996 export through the bacterial Sec pathway. *Nat Rev Microbiol* **15,** 21–36 (2017).

997 28. Calles, B., Goñi-Moreno, Á. & Lorenzo, V. Digitalizing heterologous gene expression
998 in Gram-negative bacteria with a portable ON/OFF module. *Mol Syst Biol* **15,**
999 e8777 (2019).

1000 29. Silva-Rocha, R., Martínez-García, E., Calles, B., Chavarría, M., Arce-Rodríguez, A.,
1001 Heras, A. de las, Páez-Espino, D. A., Durante-Rodríguez, G., Kim, J., Nikel, P. I.,
1002 Platero, R. & Lorenzo, V. de. The Standard European Vector Architecture (SEVA): a
1003 coherent platform for the analysis and deployment of complex prokaryotic
1004 phenotypes. *Nucleic Acids Res* **41,** D666–D675 (2013).

1005 30. Martínez-García, E., Fraile, S., Algar, E., Aparicio, T., Velázquez, E., Calles, B., Tas, H.,
1006 Blázquez, B., Martín, B., Prieto, C., Sánchez-Sampedro, L., Nørholm, M. H. H.,
1007 Volke, D. C., Wirth, N. T., Dvořák, P., Alejaldre, L., Grozinger, L., Crowther, M., Goñi-
1008 Moreno, A., Nikel, P. I., Nogales, J. & De Lorenzo, V. SEVA 4.0: an update of the
1009 Standard European Vector Architecture database for advanced analysis and
1010 programming of bacterial phenotypes. *Nucleic Acids Res* **51,** D1558–D1567 (2023).

1011 31. Nikel, P. I., Benedetti, I., Wirth, N. T., de Lorenzo, V. & Calles, B. Standardization of
1012 regulatory nodes for engineering heterologous gene expression: a feasibility study.
1013 *Microb Biotechnol* **15,** 2250–2265 (2022).

1014 32. Winsor, G. L., Griffiths, E. J., Lo, R., Dhillon, B. K., Shay, J. A. & Brinkman, F. S. L.
1015 Enhanced annotations and features for comparing thousands of *Pseudomonas*
1016 genomes in the *Pseudomonas* genome database. *Nucleic Acids Res* **44,** D646–D653
1017 (2016).

1018 33. Boratyn, G. M., Camacho, C., Cooper, P. S., Coulouris, G., Fong, A., Ma, N., Madden,
1019 T. L., Matten, W. T., McGinnis, S. D., Merezhuk, Y., Raytselis, Y., Sayers, E. W., Tao, T.,
1020 Ye, J. & Zaretskaya, I. BLAST: a more efficient report with usability improvements.
1021 *Nucleic Acids Res* **41,** W29–W33 (2013).

1022 34. Letunic, I., Doerks, T. & Bork, P. SMART: Recent updates, new developments and
1023 status in 2015. *Nucleic Acids Res* **43,** D257–D260 (2015).

1024 35. Finn, R. D., Coggill, P., Eberhardt, R. Y., Eddy, S. R., Mistry, J., Mitchell, A. L., Potter,
1025 S. C., Punta, M., Qureshi, M., Sangrador-Vegas, A., Salazar, G. A., Tate, J. &
1026 Bateman, A. The Pfam protein families database: towards a more sustainable
1027 future. *Nucleic Acids Res* **44,** D279–D285 (2016).

1028 36. Wang, J., Chitsaz, F., Derbyshire, M. K., Gonzales, N. R., Gwadz, M., Lu, S., Marchler,
1029 G. H., Song, J. S., Thanki, N., Yamashita, R. A., Yang, M., Zhang, D., Zheng, C.,
1030 Lanczycki, C. J. & Marchler-Bauer, A. The conserved domain database in 2023.
1031 *Nucleic Acids Res* **51,** D384–D388 (2023).

1032 37. Krogh, A., Larsson, B., Von Heijne, G. & Sonnhammer, E. L. L. Predicting
1033 transmembrane protein topology with a hidden markov model: application to
1034 complete genomes. *J Mol Biol* **305,** 567–580 (2001).

1035 38. Tamura, K., Stecher, G. & Kumar, S. MEGA11: Molecular Evolutionary Genetics
1036 Analysis Version 11. *Mol Biol Evol* **38,** 3022–3027 (2021).

1037 39. Jones, D. T., Taylor, W. R. & Thornton, J. M. The rapid generation of mutation data
1038 matrices from protein sequences. *Comput Appl Biosci* **8,** 275–282 (1992).

1039 40. Letunic, I. & Bork, P. Interactive Tree Of Life (iTOL) v4: recent updates and new
1040 developments. *Nucleic Acids Res* **47,** W256–W259 (2019).

1041 41. van Kempen, M., Kim, S. S., Tumescheit, C., Mirdita, M., Lee, J., Gilchrist, C. L. M.,
1042 Söding, J. & Steinegger, M. Fast and accurate protein structure search with
1043 Foldseek. *Nat Biotechnol* **42,** 243–246 (2024).

1044 42. Madeira, F., Madhusoodanan, N., Lee, J., Eusebi, A., Niewielska, A., Tivey, A. R. N.,
1045 Lopez, R. & Butcher, S. The EMBL-EBI Job Dispatcher sequence analysis tools
1046 framework in 2024. *Nucleic Acids Res* **52,** W521–W525 (2024).

1047 43. Meng, E. C., Goddard, T. D., Pettersen, E. F., Couch, G. S., Pearson, Z. J., Morris, J. H.
1048 & Ferrin, T. E. UCSF ChimeraX: Tools for structure building and analysis. *Protein*
1049 *Science* **32,** e4792 (2023).

1050 44. Montal, M. & Mueller, P. Formation of Bimolecular Membranes from Lipid
1051 Monolayers and a Study of Their Electrical Properties. *Proceedings of the National*
1052 *Academy of Sciences* **69,** 3561–3566 (1972).

1053 45. Morein, S., Andersson, A.-S., Rilfors, L. & Ran Lindblom, G. Wild-type *Escherichia*
1054 *coli* Cells Regulate the Membrane Lipid Composition in a 'Window' between Gel
1055 and Non-lamellar Structures*. *J Biol Chem* **271,** 6801–6809 (1996).

1056 46. Alcaraz, A., Nestorovich, E. M., López, M. L., García-Giménez, E., Bezrukov, S. M. &
1057 Aguilella, V. M. Diffusion, exclusion, and specific binding in a large channel: A study
1058 of OmpF selectivity inversion. *Biophys J* **96,** 56–66 (2009).

1059 47. Effect, T. H. E., Sodium, O. F., Activity, E. & The, O. F. Laboratory, University. 37–77
1060 (1948).

1061 48. Miyata, S. T., Kitaoka, M., Brooks, T. M., McAuley, S. B. & Pukatzki, S. *Vibrio*
1062 *cholerae* Requires the Type VI Secretion System Virulence Factor VasX To Kill
1063 *Dictyostelium discoideum*. *Infect Immun* **79,** 2941–2949 (2011).

1064 49. Dong, T. G., Ho, B. T., Yoder-Himes, D. R. & Mekalanos, J. J. Identification of T6SS-
1065 dependent effector and immunity proteins by Tn-seq in *Vibrio cholerae*. *Proc Natl*
1066 *Acad Sci U S A* **110,** 2623–2628 (2013).

1067 50. Miyata, S. T., Unterweger, D., Rudko, S. P. & Pukatzki, S. Dual Expression Profile of
1068 Type VI Secretion System Immunity Genes Protects Pandemic *Vibrio cholerae*. *PLoS*
1069 *Pathog* **9,** e1003752 (2013).

1070 51. Sockolosky, J. T. & Szoka, F. C. Periplasmic production via the pET expression
1071 system of soluble, bioactive human growth hormone. *Protein Expr Purif* **87,** 129–
1072 135 (2013).

1073 52. Buller, G. M., Bradford, J. A., Liu, J. & Godfrey, W. L. Novel Reagents for the
1074 Addition of Viability Measurements to Immunostaining Using Flow Cytometry.
1075 *Blood* **108,** 3879–3879 (2006).

1076 53. Winkel, J. D. te, Gray, D. A., Seistrup, K. H., Hamoen, L. W. & Strahl, H. Analysis of
1077 antimicrobial-triggered membrane depolarization using voltage sensitive dyes.
1078 *Front Cell Dev Biol* **4,** 29 (2016).

1079 54. Smart, O. S., Goodfellow, J. M. & Wallace, B. A. The pore dimensions of gramicidin
1080 A. *Biophys J* **65,** 2455–2460 (1993).

1081 55. Andersen, O. S., Koeppe II, R. E. & Roux, B. in *Biological Membrane Ion Channels*
1082 (ed. Springer New York) 33–80 (Springer, New York, NY, 2007). doi:10.1007/0-387-
1083 68919-2_2

1084 56. Queralt-Martín, M., López, M. L., Aguilella-Arzo, M., Aguilella, V. M. & Alcaraz, A.
1085 Scaling Behavior of Ionic Transport in Membrane Nanochannels. *Nano Lett* **18,**
1086 6604–6610 (2018).

1087 57. Aguilella, V. M., Queralt-Martín, M., Aguilella-Arzo, M. & Alcaraz, A. Insights on the
1088 permeability of wide protein channels: measurement and interpretation of ion
1089 selectivity. *Integrative Biology* **3,** 159–172 (2011).

1090 58. Alcaraz, A., Nestorovich, E. M., López, M. L., García-Giménez, E., Bezrukov, S. M. &
1091 Aguilella, V. M. Diffusion, exclusion, and specific binding in a large channel: a study
1092 of OmpF selectivity inversion. *Biophys J* **96,** 56–66 (2009).

1093 59. Hille, B. *Ion Channels of Excitable Membranes*. (Sinauer Associates, Inc, 2001).

1094 60. Park, H. B., Kamcev, J., Robeson, L. M., Elimelech, M. & Freeman, B. D. Maximizing
1095 the right stuff: The trade-off between membrane permeability and selectivity.
1096 *Science (1979)* **356,** 1138–1148 (2017).

1097 61. Hodgkin, A. L. & Katz, B. The effect of sodium ions on the electrical activity of the
1098 giant axon of the squid. *J Physiol* **108,** 37–77 (1949).

1099 62. Mansfield, J., Genin, S., Magori, S., Citovsky, V., Sriariyanum, M., Ronald, P., Dow,
1100 M., Verdier, V., Beer, S. V., Machado, M. A., Toth, I., Salmond, G. & Foster, G. D. Top
1101 10 plant pathogenic bacteria in molecular plant pathology. *Mol Plant Pathol* **13,**
1102 614–629 Preprint at https://doi.org/10.1111/j.1364-3703.2012.00804.x (2012)

1103 63. Mariano, G., Trunk, K., Williams, D. J., Monlezun, L., Strahl, H., Pitt, S. J. &
1104 Coulthurst, S. J. A family of Type VI secretion system effector proteins that form
1105 ion-selective pores. *Nat Commun* **10,** 5484 (2019).

1106 64. Halvorsen, T. M., Schroeder, K. A., Jones, A. M., Hammarlöf, D., Low, D. A.,
1107 Koskiniemi, S. & Hayes, C. S. Contact-dependent growth inhibition (CDI) systems
1108 deploy a large family of polymorphic ionophoric toxins for inter-bacterial
1109 competition. *PLoS Genet* **20,** e1011494 (2024).

1110 65. Bernal, P., Llamas, M. A. & Filloux, A. Type VI secretion systems in plant-associated
1111 bacteria. *Environ Microbiol* **20,** 1–15 (2018).

1112 66. Bourigault, Y., Dupont, C. A., Desjardins, J. B., Doan, T., Bouteiller, M., Le Guenno,
1113 H., Chevalier, S., Barbey, C., Latour, X., Cascales, E. & Merieau, A. *Pseudomonas*
1114 *fluorescens* MFE01 delivers a putative type VI secretion amidase that confers
1115 biocontrol against the soft-rot pathogen *Pectobacterium atrosepticum*. *Environ*
1116 *Microbiol* **25,** 2564–2579 (2023).

1117 67. Cassan, F. D., Coniglio, A., Amavizca, E., Maroniche, G., Cascales, E., Bashan, Y. &
1118 de-Bashan, L. E. The *Azospirillum brasilense* Type VI secretion system promotes
1119 cell aggregation, biocontrol protection against phytopathogens and attachment to
1120 the microalgae *Chlorella sorokiniana*. *Environ Microbiol* **23,** 6257–6274 (2021).

1121 68. Boak, E. N., Kirolos, S., Pan, H., Pierson, L. S. & Pierson, E. A. The Type VI Secretion
1122 Systems in Plant-Beneficial Bacteria Modulate Prokaryotic and Eukaryotic
1123 Interactions in the Rhizosphere. *Front Microbiol* **13,** 843092 (2022).

1124 69. Durán, D., Bernal, P., Vazquez-Arias, D., Blanco-Romero, E., Garrido-Sanz, D.,
1125 Redondo-Nieto, M., Rivilla, R. & Martín, M. *Pseudomonas fluorescens* F113 type VI
1126 secretion systems mediate bacterial killing and adaption to the rhizosphere
1127 microbiome. *Sci Rep* **11,** 5772 (2021).

1128 70. Marchi, M., Boutin, M., Gazengel, K., Rispe, C., Gauthier, J., Guillerm-Erckelboudt,
1129 A., Lebreton, L., Barret, M., Daval, S. & Sarniguet, A. Genomic analysis of the

1130 biocontrol strain *Pseudomonas fluorescens* Pf29Arp with evidence of T3SS and
1131 T6SS gene expression on plant roots. *Environ Microbiol Rep* **5,** 393–403 (2013).

1132 71. Kan, Y., Zhang, Y., Lin, W. & Dong, T. Differential plant cell responses to *Acidovorax*
1133 *citrulli* T3SS and T6SS reveal an effective strategy for controlling plant-associated
1134 pathogens. *mBio* **14,** e0045923 (2023).

1135 72. Reyes-Pérez, P. J., Jiménez-Guerrero, I., Sánchez-Reina, A., Civantos, C., Moreno-de
1136 Castro, N., Bernal, P. & Pérez-Montaño, F. The type VI secretion system of
1137 *Sinorhizobium fredii* USDA257 is required for a successful symbiosis with *Glycine*
1138 *max* cv Pekin. *bioRxiv* doi: 10.1101/2023.12.14.571490 (2024).
1139 doi:10.1101/2023.12.14.571490

1140

1141